博士論文

Numerical modeling on combustion behaviors in a hydrocarbon fueled scramjet combustor

(炭化水素を燃料とするスクラムジェット
燃焼器における燃焼挙動に関する数値解析)

崔　敏鎬

Acknowledgements

Contents

List of Tables

List of Figures

Abbreviations

AUSM   **A**dvection **u**pstream **s**plitting **m**ethod

CFL   **C**ourant **F**reidrich **L**ewy

DNS   **D**irect **n**umerical **s**imulation

FD, **FDM**   **F**inite **d**ifference (**m**ethod)

FDS   **F**lux **d**ifference **s**plitting

FV, **FVM**   **F**inite **v**olume (**m**ethod)

FVS   **F**lux **v**ector **s**plitting

LES   **L**arge **e**ddy **s**imulation

MUSCL   **M**onotonic **u**pstream-centered **s**cheme for **c**onservation **l**aws

PDE   **P**artial **d**ifferential **e**quation

PDF   **P**robability **d**ensity **f**unction

PLIF   **P**lanar **l**aser-**I**nduced **F**luorescence

RANS   **R**eynolds-**a**veraged **N**avier-**S**tokes equations

Scramjet   **S**upersonic **c**ombustion **ramjet**

TVD   **T**otal **v**ariation **d**iminishing

Physical Constants and Parameters

Universal gas constant	R	$=$	$8.314\,462\,1\,\mathrm{J/(mol\,K)}$
		$=$	$1.987\,204\,1\,\mathrm{cal/(mol\,K)}$
Turbulent Prandtl number	Pr	$=$	0.600
Turbulent Schmidt number	Sc	$=$	0.600
AUSM parameters	α	$=$	0.1875
	β	$=$	0.125

TABLE 1: Physical quantities of participating chemical species

Species	Molar mass (kg/mol)	Collision diameter (nm)	Effective temperature (K)
H_2	2.0158×10^{-3}	2.920×10^{-1}	38.00
H	1.0079×10^{-3}	2.310×10^{-1}	38.41
O_2	31.9988×10^{-3}	3.458×10^{-1}	107.40
H_2O	18.0152×10^{-3}	2.605×10^{-1}	572.40
H_2O_2	34.0146×10^{-3}	3.020×10^{-1}	33.09
CH_4	16.0423×10^{-3}	3.750×10^{-1}	140.00
CH_3	15.0344×10^{-3}	3.190×10^{-1}	38.27
CO	28.0101×10^{-3}	3.650×10^{-1}	98.00
CO_2	44.0095×10^{-3}	3.760×10^{-1}	244.00
HCO	29.0180×10^{-3}	3.080×10^{-1}	71.21
$HCHO$	30.0259×10^{-3}	3.080×10^{-1}	71.21
N_2	28.0134×10^{-3}	3.621×10^{-1}	97.53

Symbols

Symbol	Meaning	Unit
c	concentration	mol/m^3
e_t	total internal energy	J
f	body force acceleration	m/s^2
h_t	total enthalpy	J
J	momentum ratio between main flow and fuel injection	*dimensionless*
m	mass	kg
M	molar mass	kg/mol
N	number of species	*dimensionless*
p	pressure	Pa
t	time	s
T	temperature	K
$\vec{u}$	velocity	m/s
u, v, w	velocity components	m/s
V	diffusion velocity	m/s
w, Y	mass fraction	*dimensionless*
X	mole fraction	*dimensionless*
η_{mix}	mixing efficiency	*dimensionless*
η_{comb}	combustion efficiency	*dimensionless*
λ	bulk viscosity	kg/(m s)
ρ	density	kg/m^3
$\bar{\bar{\sigma}}$	stress	Pa
$\bar{\bar{\tau}}$	deviatoric stress	Pa
μ	dynamic viscosity	kg/(m s)

ν	kinematic viscosity	m^2/s
ν_t	subgrid scale viscosity	m^2/s

Chapter 1

Introduction

For research and development of reliable scramjet engine, deep understandings of physical phenomena occurring in the combustor are required. Effect of supersonic and turbulent flow characteristics mainly determines combustion behavior, while in-time mixing and chemical reaction enables efficient and controllable combustion in a limited sized engine. From these facts one can realize that thorough understanding on how those factors can affect operation of the engine is mandatory for satisfactory hypersonic vehicle building. Especially hydrocarbon fueled engine research is not addressed as much as hydrogen counterpart. Since hydrocarbon fuels are more applicable, versatile and safer at treatment than hydrogen, research on hydrocarbon fueled scramjet engine is urgent.

In order to conduct a research for that, fluid dynamics / combustion theoretical approach, experiment on high enthalpy wind tunnel, computational simulation, or combination of above would be an appropriate method. Experimental method is a primary option for scramjet research owing to its reliability. Numerical method can be applied to obtain detailed and convoluted data which can maximize experimental results. The

portion of researches using numerical method is increasing owing to its recent enhancement in fluid mechanics and chemistry field. Specifically, present numerical scramjet researches commonly deal with hydrogen fuel which has simple reaction steps. To extend current research area it is required to study hydrocarbon fuels with numerical method.

1.1 Background

A brief explanation about usage of scramjet engine and principles of its combustor will be given in this section. Readers are advised to understand those basic facts in order to address problems of the thesis.

1.1.1 Hypersonic flight powered by a scramjet engine

In the field of future aerospace engineering development, there is and would be a continuously expanding demand for civil, military and space hypersonic flight mission. Although it is a common knowledge that we currently have limited number of supersonic transportation services, hypersonic air routes would attract attention in the future matured market along with the growth of the economies and rise of value of time in context of transport economics. In the applications of surveillance and missile, the hypersonic aircraft can attract a great interest. US Air Force SR-71 already proved effectiveness of high-speed reconnaissance airplane by its successful services. When it competes with satellites, it is advantageous to them due to rapid operation response capability. Space tourism also attracts attention from enterprises as a rising future business model.

Up to the present time, a variety of propulsion systems for a high-speed vehicle have been developed. Some of them are realized and widely utilized, whereas some of

them are yet staying as a conceptual idea or being tested in laboratory. Among them, an air-breathing jet engine is one of the most versatile propulsion system for the flight in the atmosphere. When it is compared to a rocket engine, which can generate thrust at all speeds, the air-breathing engine is favorable in aspect of larger specific impulse I_{sp} to a rocket engine. Larger specific impulse means the engine could be much better fuel-economic.

The compromise is, with higher intake Mach number, performance of propeller or turbomachine gets worse. Due to Mach number effect, overall performance of the conventional jet engine is deteriorated. To overcome this, compressing the air coming into the engine with body of the vehicle itself arises as a attractive candidate. This is the idea of ramjet engine, its name came from its character of ramming the incoming air. It does not have rotating machine parts for compression and expansion processes of propellant. As the airspeed of the vehicle shifted into hypersonic flight regime, total enthalpy of the air overwhelms fuel combustion energy added. To suppress excessively high static temperature, combustion of the fuel must take place while the air flow at supersonic speed. This is supersonic combustion ramjet engine, or in short, scramjet. In theory, scramjet engine can generate substantial amount of thrust at flight Mach number of 5 to 20.

1.1.2 Scramjet engine combustor

A good combustor should be able to transfer fuel chemical energy fully into thermal energy of working fluid within limited time, while minimizing losses due to irreversible processes. Flow inside scramjet combustor is by definition supersonic, so working fluid passes by within quite short time. Generally speaking, the residence time of working fluid inside combustor ranges within 1 ms because length of the combustor is approximately

meter order and the flow speed is several hundred m/s order. This is one order of magnitude shorter than that of ordinary turbomachine jet. Within this residence time, all processes such as mixing and reaction should take place.

1.2 Technical achievements on developing a scramjet combustor

A good scramjet combustor should be able to achieve proper functionality which can be categorized into several fields stated below. At first, stable combustion is crucial to controlled flight. This requires advanced mixing and flame-holding techniques. The combustion should last at various off-design conditions such as vehicle airspeed / height / position change, thrust control, upstream nonuniformity or engine maneuvering. Also it should give efficient performance by minimizing total pressure drop and avoiding thermal choke.

A variety of approaches for mixing and flameholding are performed. As stated in previous section, completing those processes within restrained time became a big challenge in development of scramjet. To list up several proposed measurements includes effective fuel injection, enhanced interaction between the flow and shock or shear layer and passive / active flameholder devices.

Advanced fuel injection strategies are the most accessible approach for combustion control. Gruber et al.[1] investigated relation between fuel injector configurations, i.e. injection angle and shape of the hole, and mixing and penetration. They pointed out that the mechanism of mixing of freestream flow and the fuel is driven by vortices. They insisted that the size of vortex determines effectiveness of fuel mixing. Ben-Yakar et al.[2] altered fuel type and observed the difference. In case of hydrogen fuel, coherent

vortices are maintained while in case of ethylene they brake into smaller ones. They argued that the difference come from velocity difference of main flow and fuel injection. Kang et al.[3] made equivalence ratio as independent condition and found "sweet spot" of it. They also discussed how spanwise pressure gradient expedite spanwise mixing through numerical analysis.

The fuel may be injected parallel to the air flow. In that case, strut flameholder may exhibit good mixing property. Gerlinger et al.[4] tried to directly increase vorticity using distinct strut/injector structure. The lobed strut resulted in favorable mixing efficiency, while inducing large kinetic energy loss. Kim et al.[5] attempted to assess the loss by measuring total pressure. They induced shock to parallel fuel injection using mount on the wall, and revealed that the shock can enhance radial convection and elongate recirculation zone.

Cavity flameholder is another attractive device. Gruber et al.[6] investigated relation of fuel injection position and cavity flameholder funtionality as well as effect of shock train controlled by backpressure. Since the cavity is expected to supply shear layer and mass exchange should be smooth, fuel injection inside the cavity was recommended. Also they stated that integrating shear layer and shock with fuel jet gives great enhancement on mixing. Liang et al.[7] sought methods to make fuel flow meet shear layer using cavity flameholder. By injecting the fuel, the shear layer has been raised to meet main fuel plumb. Also they found that counter rotating vortex which flown into cavity works on spanwise scalar dissipation in the cavity

ignition can be achieved by several methods. Spark and/or photoradical ignition could give additional heat to a specific region of combustor.

1.3   Combustion behavior inside scramjet engine combustor

The ultimate goal of combustion behavior research is to know which physical and chemical variations affects in which mechanism. Therefore, combustion behavior should be defined as follow: While the fuel is combusted in the combustor, concrete physical and chemical processes and the factors which affects the function, controllability and efficiency of the combustion.

1.3.1   Numerical analyses for combustion behavior

RANS(Reynolds-Averaged Navier-Stokes) and LES are two representative methods which can be used for modeling turbulence which cannot be fully resolved explicitly because of large scale discrepancy in a given flow of practical combustor. Many previous numerical analyses applied RANS scheme for scramjet combustor simulation due to limited computational resources.[5] [4] [3] SST model for turbulence is popular among these researches.

However, RANS results are not sufficient to precisely simulate mixing and combustion phenomena because it lacks ability to represent unsteadiness of the flow which largely influences these phenomena. LES is capable of those unsteadiness because large eddies are directly calculated, while small eddies which are not influential on mixing and reaction. Recent researches regard LES a powerful option for combustor simulation.

Berglund and Fureby[8] conducted LES simulation for supersonic flow and combustion examination. In this research, numerical results were qualitatively comparable with experimental counterpart.

In Fureby et al.[9]'s work, For HEG(shock tunnel) flow RANS was used and for the model combustor RANS and LES was compared with experimental result. Only Fuel injector exists as a flameholder. With pressure distribution, velocity field, concentration and combustion efficiency, eligibility of RANS and LES was analyzed. RANS has shown qualitative agreement, whereas LES have shown quantitative agreement with experimental result.

1.3.2   Chemistry

Application of detailed chemistry on a numerical analysis of complex flow reactor is not practical due to limited resources. The first choice for chemical approach is to address hydrogen as fuel which has simple reaction mechanism.[5][10] One may find several attempts that applied hydrocarbon fuels. They used quite simplified methods. Compared to numerical analysis, experiments do not have limitation at kind of fuel, so there are many hydrocarbon combustion results.[6][2]

1.3.3   Factors of combustion behavior

with those results obtained the combustion behavior can be investigated effectively. The factors which determine the behavior would be parameters such as dynamic pressure ratio (and resultant penetration), equivalence ratio, injection configuration, arrangement of flameholder. Wendt et al.[11] suggested that fuel total temperature effects mixing in case of parallel injection.

1.4 Objective of the research

Numerical analysis of a scramjet combustor at the same condition with previous experiments will be performed. Detailed flow field information and mechanism of mixing/combustion processes would be obtained which could not be revealed directly by experiment. For this purpose, LES simulation will be conducted with various combustion models, and the results will be combined with experimental ones.

To the present, there has rarely been researches which directly calculated combustion of hydrocarbon along with fluid mechanics in a supersonic combustor with cavity flameholder. Therefore, A simultaneous calculation can be a milestone at supersonic combustor field. It is clear that detailed reaction mechanisms are not applicable, so the possibility has been measured by reduced reaction mechanisms.

In addition, factors and mechanisms which influences controllability of a scramjet engine will be investigated numerically based on discussions made above. Momentum ratio between main flow and fuel injection which influences penetration of the fuel and flow field structure substantially as well as fuel temperature change which is often entailed in practical scramjet engine will be altered as independent variables in order to discover which factors are changed by them and how they affect combustion behavior. Establishment of fundamental knowledge of combustor control by investigation of physical phenomena occurred by given conditions is another significant objective of this research.

Chapter 2

Theory and Numerical

Methodology

Physical phenomena in a scramjet combustor could be categorized into fluid dynamics and chemistry.

Compressible effects by a supersonic flow, turbulence by velocity gradient created by no-slip walls and stratified flow, heat transfer within the flow or between fluid and solid wall, mass diffusion of different species are representative aerodynamic phenomena. Meanwhile, species concentration change and consequential heat release or in some cases heat absorption by reaction are combustive phenomena.

An experiment can be regarded as a intuitive, simple and reliable method for analysis of a scramjet combustor. However, one may find some difficulty when trying to get enough information from an experimental apparatus as much as possible. For instance, from experiment, one can obtain just discrete distribution of velocity and/or pressure.

In contrast, by conducting numerical simulations, one can harvest satisfactory supporting data which can cooperate with experimental data. In this chapter, methodologies which can simulate these physical phenomena numerically will be described.

In order to define governing equations, physical phenomena in concern should be stated. Fundamentally, the fluid is treated as an object, so one can use Navier-Stokes equations for governing equation. Euler equation can also be the governing equation. However, Since I want to see the effect of viscosity, Euler equation is used when only verifying source code of CFD program.

The flow is consist of several species. Basically, because combustion is being occurred, There would be at least reactant and product. The reactant includes oxidizer and fuel. Air or oxygen corresponds to the oxidizer. For the type of fuel, hydrogen or hydrocarbon is the most frequent application.

conserved quantities (mass, momentum, energy) and non-conserved quantities (concentrations) are expressed by balance equations which contains temporal term, convection term along with diffusion term and source term conditionally.

2.1   Theoretical background

2.1.1   Governing equations

In order to conduct scientific research of a scramjet engine, one is required to interpret physical phenomena using mathematical expressions, which are called governing equations. In spite of apparent difference between fluid flow, transport phenomena by motion of molecules and chemical reaction, which are main phenomena taking place, they can be treated side by side by virtue of mathematical expression.

The fluid flow can depicted by a system of partial differential equations(PDE), which are derived from conservation laws of mass, momentum and energy. Those laws are described in Lagrangian way. In order to deal with those with a control volume rather than a system, those laws are formulated in Eulerian way owing to the well-known Reynolds transport theorem. Also, constitutive equation for fluids which describes relation between strain rate and stress acting on an infinitesimal volume would close momentum equation.

2.1.1.1 Continuity equation

Equation of mass conservation has another name, continuity equation. As the name indicates, this equation is derived upon assumption of continuity of the material, which enables using differential expression. Starting from mass conservation of a system,

$$\frac{dm}{dt} = 0 \tag{2.1}$$

where m is mass of a system. This equation describes mass change of a system, so in order to use with fluids, the equation should be related with a control volume. after several steps using Reynolds transport theorem, the equation becomes

$$\frac{\partial \rho}{\partial t} + \nabla \cdot (\rho \vec{u}) = 0 \tag{2.2a}$$

which describes mass conservation of a control volume. The equation is in vector notation, and it can also be expressed in tensor notation, provided that certain coordinate system is used. The following equation is expressed with Cartesian coordinate system

because computational domain which will be used later in this thesis is Cartesian.

$$\frac{\partial \rho}{\partial t} + \frac{\partial}{\partial x_j}\left(\rho u_j\right) = 0 \tag{2.2b}$$

The equation above is expressed with partial derivative. With total(i.e. substantial/-material) derivative, the equation changes into

$$\frac{D\rho}{Dt} + \rho \nabla \cdot \vec{u} = 0 \tag{2.3a}$$

using total derivative $\frac{D}{Dt}$. Again tensor notation can be applied.

$$\frac{D\rho}{Dt} + \rho \frac{\partial u_j}{\partial x_j} = 0 \tag{2.3b}$$

The first term in total derivative can be canceled in case of incompressible flow $\frac{D\rho}{Dt} = 0$.

$$\frac{\partial u_j}{\partial x_j} = 0 \tag{2.4}$$

2.1.1.2   Navier-Stokes equation

The momentum conservation equation is Navier-Stokes equation. Since momentum is a vector quantity, Navier-Stokes equation is a system of PDE if expressed in scalar. Contrast to the continuity equation, mainly due to convective terms, the equation is nonlinear. This property leads to complex solution which cannot be obtained analytically, often related with turbulence.

The equation is derived from Newton's second law of motion. After applying Reynolds' transport theorem and state all forces acting on a infinitesimal control volume, the equation below is obtained.

$$\rho \frac{\partial \vec{u}}{\partial t} + \rho \left(\vec{u} \cdot \nabla \right) \vec{u} = \nabla \cdot \bar{\bar{\sigma}} + \rho \vec{f} \tag{2.5}$$

When expressed in tensor notation, the equation is represented as

$$\rho \frac{\partial u_j}{\partial t} + \rho u_k \frac{\partial u_j}{\partial x_k} = \frac{\partial \sigma_{ij}}{\partial x_i} + \rho f_j. \tag{2.6}$$

For numerical analysis, discretization could be easier if all variables are under differential operator. with continuity equation combined,

$$\frac{\partial \left(\rho u \right)}{\partial t} + \nabla \cdot \left(\rho u \vec{u} \right) = \left(\nabla \cdot \bar{\bar{\sigma}} \right)_x + \rho f_x \tag{2.7a}$$

$$\frac{\partial \left(\rho v \right)}{\partial t} + \nabla \cdot \left(\rho v \vec{u} \right) = \left(\nabla \cdot \bar{\bar{\sigma}} \right)_y + \rho f_y \tag{2.7b}$$

$$\frac{\partial \left(\rho w \right)}{\partial t} + \nabla \cdot \left(\rho w \vec{u} \right) = \left(\nabla \cdot \bar{\bar{\sigma}} \right)_z + \rho f_z \tag{2.7c}$$

Also in tensor notation,

$$\frac{\partial}{\partial t} \left(\rho u_j \right) + \frac{\partial}{\partial x_k} \left(\rho u_k u_j \right) = \frac{\partial \sigma_{ij}}{\partial x_i} + \rho f_j \tag{2.8}$$

Here, σ is stress acting on the control volume. From definition of fluid, stress is related with rate of deformation. Most of fluids dealt with in practical engineering problems, including this thesis, are assumed to be Newtonian fluid. Owing to the definition of Newtonian fluid, One can derive constitutive equation of Navier-Stokes equation, which connects dynamics and kinematics.

$$\sigma_{ij} = -p \delta_{ij} + \lambda \frac{\partial u_k}{\partial x_k} \delta + 2 \mu D_{ij} \tag{2.9}$$

where

$$d_{ij} = \frac{1}{2} \left(\frac{\partial u_j}{\partial x_i} + \frac{\partial u_i}{\partial x_j} \right) \tag{2.10}$$

p in this equation represents normal stress which is not directly related with rate of deformation. Consequently, that is pressure when the fluid is in rest, and thermodynamic pressure which appears in equation of state of a gas. In contrast, mechanical pressure $\bar{p}$ is defined to be trace of stress tensor. They are in general not the same.

Coefficient μ is (dynamic) viscosity. It is a thermodynamic property, which means it is dependent on other thermodynamic quantities. During computational analysis of combustion, viscosity should be calculated at each moment, each part of the system.

After rearranging, one can confirm that the quantity $\lambda + \frac{2}{3}\mu$ appears with rate of dilatation $\frac{\partial u_k}{\partial x_k}$. therefore, it is natural to define $\lambda + \frac{2}{3}\mu$ as bulk viscosity.

To satisfy the second law of thermodynamics, those viscosities should be non-negative. Stokes assumed this coefficient to be zero. And it is known to be valid for monatomic gases. Due to difficulties in measurement, values of all fluids are not known exactly. Although working fluid of this research is polyatomic, it does not violate physics extensively to assume that bulk viscosity is zero. It can be formally compared with inviscid assumption. CFD code disregarded effect of it. However, for precise physics in waves where high dilatation occurs, it is preferable to take appropriate assumption into consideration.

Substituting 2.9 into 2.8, one can obtain detailed Navier-Stokes equation.

$$\frac{\partial}{\partial t}\left(\rho u_j\right) + \frac{\partial}{\partial x_k}\left(\rho u_k u_j\right) = -\frac{\partial p}{\partial x_j} - \frac{\partial}{\partial x_j}\left(\lambda\frac{\partial u_k}{\partial x_k}\right) + \frac{\partial}{\partial x_i}\left(\mu\left(\frac{\partial u_i}{\partial u_j} + \frac{\partial u_j}{\partial x_i}\right)\right) + \rho f_j$$

$$= -\frac{\partial p}{\partial x_j} - \frac{\partial}{\partial x_j}\left(\lambda\frac{\partial u_k}{\partial x_k}\right) + \frac{\partial}{\partial x_i}\left(\mu\left(\frac{\partial u_i}{\partial u_j} + \frac{\partial u_j}{\partial x_i}\right)\right) + \rho f_j$$

$$(2.11)$$

2.1.1.3   Energy equation

Energy equation is the 1st law of thermodynamics, which represents the conservation of energy.

Here, internal energy, and consequentially total enthalpy include both sensible energy which is related to temperature and chemical energy which is related to chemical species. Also, it is dependent upon composition of consisting species. Therefore, any source term which represents chemical reaction becomes unnecessary.

$$\frac{\partial\left(\rho e_t\right)}{\partial t} + \nabla\cdot\left(\rho\vec{u}h_t\right) = -\nabla\cdot\left(-\lambda\nabla T + \rho\sum_{k=1}^{N}h_k Y_k\vec{V}_k\right) + \nabla\cdot\left(\bar{\bar{\tau}}\cdot\vec{u}\right) \qquad (2.12)$$

Or in tensor notation,

$$\frac{\partial\left(\rho e_t\right)}{\partial t} + \frac{\partial}{\partial x_k}\left(\rho u_k h_t\right) = -\frac{\partial}{\partial x_i}\left(-\lambda\frac{\partial T}{\partial x_i} + \rho\sum_{k=1}^{N}h_k Y_k V_{k,i}\right) + \frac{\partial}{\partial x_j}\left(\tau_{ij}u_j\right) \qquad (2.13)$$

2.1.1.4   Chemical species balance equation

Since chemical species is not a conserved quantity, the equation cannot be named a conservation equation. However, with support of a source term, chemical phenomena can be expressed with temporal term, convection term, diffusion term and source term,

which is a balance equation.

$$\frac{\partial (\rho Y_k)}{\partial t} + \nabla \cdot \left(\rho \left(\vec{u} + \vec{V}_k \right) Y_k \right) = \dot{\omega}_k \tag{2.14}$$

$$\frac{\partial (\rho Y_k)}{\partial t} + \frac{\partial}{\partial x_i} \left(\rho \left(u_i + V_{k,i} \right) Y_k \right) = \dot{\omega}_k \tag{2.15}$$

2.1.2 Transport phenomena

Transport phenomena are occurred by random motion of molecules, which are irreversible and diffusive. By the term diffusive it means all governing equations of transport phenomena are represented as parabolic PDEs. momentum, energy and each species with gradient would diffuse.

2.1.2.1 Species diffusion

In equation 2.15, V_k stands for diffusion velocity. If there are only two species in the mixture, the diffusion velocity can be obtained from Fick's law. In contrast, for multi-species mixture, full equations for diffusion velocities form complex system which is quite costly. Therefore Hirschfelder and Curtiss approximation has been used for the diffusion velocity calculation.[12] This approximation would fall back to Fick's law in case of binary diffusion calculation, and quite convenient for multi-species cases.

$$\begin{aligned} V_{k,i} &= \rho D_k \frac{1}{Y_k} \frac{M_k}{M} \frac{\partial X_k}{\partial x_i} \\ &= \rho D_k \frac{1}{X_k} \frac{\partial X_k}{\partial x_i} \end{aligned} \qquad \text{for} \quad k = 1, N \tag{2.16}$$

Summing all equations up results in continuity equation, which leads to overdetermined system of equation. In order to avoid over-determination, compensation velocity can be

introduced. Then the equations for diffusion velocity will be

$$V_{k,i}Y_k = \rho D_k \frac{M_k}{M} \frac{\partial X_k}{\partial x_i} - \rho \sum_{l=1}^{N} D_l \frac{M_l}{M} \frac{\partial X_l}{\partial x_i} \qquad \text{for} \quad k = 1, N \qquad (2.17)$$

2.1.2.2 viscosity

The first term on the right side of equation 2.8 is stress term. Stress in a newtonian fluid is proportional to the rate of strain change. The equation explaining this relation is constitutive equation for fluid.

$$\sigma_{ij} = -p\delta_{ij} + \lambda\delta_{ij}\frac{\partial u_k}{\partial x_k} + \mu\left(\frac{\partial u_i}{\partial x_j} + \frac{\partial u_j}{\partial x_i}\right) \qquad (2.18)$$

where λ and μ are respectively second(or volume or bulk) viscosity and dynamic viscosity. The second viscosity is assumed to be $-2/3\mu$. This assumption corresponds to the case of monoatomic gas or incompressible flow. That is, there is no difference between mechanical pressure which can be defined as trace of stress tensor and thermodynamic pressure which is in equation of state.

2.1.2.3 Heat conduction

By definition, heat transfer mainly originates from gradient of temperature. heat may be transferred by concentration gradient, which is called Dufour effect. This effect can be neglected in combustion process, so do in this research.

$$\vec{q} = -\lambda\nabla T + \rho \sum_{k=1}^{N} h_k Y_k \vec{V}_k \qquad (2.19)$$

$$q_i = -\lambda\frac{\partial T}{\partial x_i} + \rho \sum_{k=1}^{N} h_k Y_k V_{k,i} \qquad (2.20)$$

When internal energy defined in energy conservation equation includes chemical energy, energy flux due to species diffusion should be accounted for as well. The second term in the right side of equations above corresponds to this effect.

2.1.3   Turbulence Modeling

For a proper simulation of fluid dynamics in a scramjet combustor, turbulence should be considered properly. The average main flow velocity in the combustor reaches more than $1000 \, \mathrm{m/s}$, while combustor length scale (e.g. hydraulic diameter) is not so small order of $0.1 \, \mathrm{m}$. Then Reynolds number of the flow would be an order of 10^6 to 10^8. Therefore The flow in a scramjet combustor is thought to be fully turbulent.

In order to carry a proper simulation out, All scales those can be represented in the case should be resolved in the simulation. For turbulence, we have from Kolmogorov scale which is the smallest to the integral scale which is the largest. DNS is capable of all these scales and would produce an exact and precise result. In this case, Kolmogorov length scale can be calculated roughly. With size of the largest eddies being an order of $10 \, \mathrm{mm}$, kinematic viscosity being an order of $10 \times 10^{-5} \, \mathrm{m^2/s}$ and jet velocity an order of $10 \times 10^3 \, \mathrm{m/s}$, Kolmogorov length scale from turbulence similarity theory will be $\frac{\nu^3 \delta^{1/4]}}{v^3} \sim 0.03 \, \mathrm{mm}$. With given size of combustor, DNS is unfortunately impractical for scramjet combustor simulation. Therefore, modeling of the smaller scales should be applied with acceptable computational cost. In this research, large-eddy simulation is used because it is superior at capturing flame structure.

LES is an abbreviation of Large Eddy Simulation. As its name explains, LES deals with large eddies directly, while small eddies are modeled. It can be compared with DNS and RANS. Direct Numerical Simulation solves Navier-Stokes equation and other governing equations directly. This implies that all phenomena occurred at various

and wide range of scales in both time and space are directly simulated. In proper DNS, if a flow is turbulent, there will be largest and smallest eddy scale, and all scales between them should be captured within calculation domain. In case of RANS, there is no limitation on the size of mesh used for calculation because all small scale phenomena are all modeled. In contrast, LES assumes that large eddies are directly calculated while small ones are modeled. Therefore how large or small eddies are to be covered should be considered in order for proper LES.

In LES, variables are filtered in spectral or physical space. After filtering, the governing equation changes into the equation below.

$$\text{Mass:} \quad \frac{\partial \bar{\rho}}{\partial t} + \frac{\partial}{\partial x_j} \left(\bar{\rho} \tilde{u}_j \right) = 0 \tag{2.21}$$

$$\text{Momentum:} \quad \frac{\partial}{\partial t} \left(\bar{\rho} \tilde{u}_j \right) + \frac{\partial}{\partial x_k} \left(\bar{\rho} \tilde{u}_k \tilde{u}_j \right) = \frac{\partial \bar{\sigma}_{ij}}{\partial x_i} - \frac{\partial}{\partial x_i} \left(\bar{\rho} \left(\widetilde{u_i u_j} - \tilde{u}_i \tilde{u}_j \right) \right) + \rho \bar{f}_j \tag{2.22}$$

$$\text{Energy:} \quad \frac{\partial \left(\bar{\rho} \tilde{e}_t \right)}{\partial t} + \frac{\partial}{\partial x_k} \left(\bar{\rho} \tilde{u}_k \tilde{h}_t \right) = \frac{\partial}{\partial x_i} \left(\overline{\lambda \frac{\partial T}{\partial x_i}} - \overline{\rho \sum_{k=1}^{N} h_k Y_k V_{k,i}} \right) \tag{2.23}$$

$$- \frac{\partial}{\partial x_i} \left[\bar{\rho} \left(\widetilde{u_i h_s} - \tilde{u}_i \tilde{h}_s \right) \right] + \overline{\frac{\partial}{\partial x_j} \left(\tau_{ij} u_j \right)}$$

$$\text{Species:} \quad \frac{\partial \left(\bar{\rho} \tilde{Y}_k \right)}{\partial t} + \frac{\partial}{\partial x_i} \left(\bar{\rho} \tilde{u}_i \tilde{Y}_k + \bar{\rho} \overline{V_{k,i} Y_k} + \bar{\rho} \left(\widetilde{u_i Y_k} - \tilde{u}_i \tilde{Y}_k \right) \right) = \bar{\omega}_k \tag{2.24}$$

Latter 3 equations now contain additional flux terms, which cannot be solved thus should be modeled. In practice, the flux term in chemical species equation is often neglected.

Kolmogorov's theory provides that turbulent scales are distributed in energy cascade and kinetic energy contained in eddies can be dissipated into heat by viscosity at the lowest scale range only. Then overall cascade can be postulated, and consequently,

smaller scales can be modelled with simple formulation or similarity analysis which involves filtering of the flow field.

Smagorinsky model has been used in this research. The unresolved Reynolds stresses are expressed as below.

$$
\mathcal{T}_{ij} - \frac{\delta_{ij}}{3}\mathcal{T}_{kk} = -\nu_t \left(\frac{\partial \tilde{u}_i}{\partial x_j} + \frac{\partial \tilde{u}_j}{\partial x_i} - \frac{2}{3}\delta_{ij}\frac{\partial \tilde{u}_k}{\partial x_k} \right) = -2\nu_t \left(\tilde{S}_{ij} - \frac{\delta_{ij}}{3}\tilde{S}_{kk} \right) \tag{2.25}
$$

Here, subgrid scale viscosity ν_t is modeled as

$$
\nu_t = (C_S\Delta)^2 \left| \tilde{S} \right| = (C_S\Delta)^2 \left(2\tilde{S}_{ij}\tilde{S}_{ij} \right)^{1/2} \tag{2.26}
$$

This model assumes that the eddies below subgrid scale are isotropic, which is reasonable in many cases. However, several flow does not satisfy this assumption. For example, Turbulence near no-slip wall is highly directional. If this flow feature comes into serious consideration, alternative modeling such as dynamic subgrid scale eddy viscosity model[13] may be helpful.

2.2 Numerical methodology

2.2.1 Finite difference method

All governing equations given above are differential equations. Converting them into algebraic equations enables numerical analysis. All first-order differential operator is to be difference of numerical flux.

$$
\frac{\partial u}{\partial x} = \frac{u_{j+1/2} - u_{j-1/2}}{\Delta x} \tag{2.27}
$$

This is basic approach in finite difference method.

All numerical method can be substituted into specific definition of the flux. The definition can be shared between FVM and FDM. The expression above is suitable for FDM.

2.2.2 Upwind scheme

In general, central difference scheme shows best accuracy at a given number of stencil. However, Navier-Stokes equation requires upwind spatial discretization techniques for capability of capturing discontinuities, which is created by shock wave or species contact. Advection upstream splitting method(AUSM)[14] is the upwind scheme for this research due to its many advantages over Flux Difference Splitting[15] or Flux Vector Splitting[16]. While this scheme maintaining sharpness of Roe's FDS, it is free from need for obtaining complicated Jacobian matrix of convection term.

AUSM has been developed in decades by a variety of researchers[17] [18], and there are several variations of it. AUSM+-up for all speeds[19] which has been developed from AUSM+Liou[20] has been chosen for present work.

With AUSM, convection term in the PDE is divided into advection term and pressure term. Those terms are calculated with modified speed of sound and corresponding Mach number.

2.2.3 High-order difference method

Navier-Stokes equation is categorized as a hyperbolic partial differential equation. Solving this kind of equation with central difference method naturally produces spurious solution near discontinuity. Since a supersonic flow may contain weak solutions,

Numerical flux can be expressed with values in its stencil as below.

$$u_i^{n+1} = \sum_k c_k u_{i+k}^n \tag{2.28}$$

In general, in order to gain sharper and preciser solution should be adapted high-order difference method. Unfortunately, The well-known Godunov's law indicates that linear difference method which is higher than first order would produce a spurious oscillating solution if the solution contains discontinuities. In order to evade this trap, the method should be nonlinear. A good systematic approach is to adjust the numerical flux by multiplying flux limit. The flux limit can be defined by certain criteria.

Prior to the suggestion of flux limits, total variation diminishing(TVD) condition will be explained. TVD stands for the method that does not increase sum of variation of the variable. That is,

$$\sum \left| u^{i+1} - u^i \right| \leq \sum \left| u^i - u^{i-1} \right| \tag{2.29}$$

If TVD is satisfied, then the method consequently satisfies monotonicity preserving feature.[21] In order to satisfy this condition, the flux limit should be in the TVD region

2.2.4 Temporal difference

The first term in the equations represents temporal change of the quantities. Those are solved by time marching. This is the same with solving ODE with initial condition. From the present state, calculate the future state of which difference shown in discretization of temporal change term. To calculate this term numerically, it should be discretized with an appropriate method out of many candidates. Those methods could be categorized by different level of precision and stability.

Stability of a method is highly dependent upon whether the method is explicit or implicit. Those corresponds to forward and backward numerical differentiation, respectively. Explicit methods use terms between ith and the next $(i+1)$th terms.

$$\frac{\partial u}{\partial t} = \frac{f\left(u^i, u^{i+1}, \cdots\right)}{\Delta t} \tag{2.30}$$

Similarly implicit methods can be expressed except the fact that the terms between $(i-1)$th and ith terms.

$$\frac{\partial u}{\partial t} = \frac{f\left(u^i, u^{i-1}, \cdots\right)}{\Delta t} \tag{2.31}$$

Variables belong to the terms other than temporal term has ith state value. Explicit methods have stability issue when used with hyperbolic PDE, which belongs to governing equations for supersonic flow. However, explicit method can be implemented at hand and requires less computational resources. In order to suppress divergence, time step should be given within certain value. Ratio between smallest grid size and the time step is the limiting condition. This is called CFL condition, which ranges between 1 to 3 depending on the method used.

Meanwhile, implicit methods usually do not diverge with any given length of time step. it consumes much more resources compared to explicit method, and hard to implement. If stiffness of the system matters, however, implicit method could be much faster. LU-SGS[22] is widely accepted representative implicit method.

Lower order difference methods tend to produce phase lag and modified amplitude in their solution. To overcome those error, higher precision difference methods are preferred. The most popular method is Runge-Kutta method. The precision can be determined following the problem demands, and those are readily induced.

In this thesis, all results obtained are calculated by explicit first order precise solutions. CFL condition is maintained below 0.4 in most cases. Since calculation of chemical reaction is included, the time step limitation was not that harsh.

Chapter 3

Comparison on chemical reaction models applied for scramjet combustor

3.1 Introduction

Performing a successful numerical analysis of a scramjet engine combustor requires adequate modelings for physical phenomena occurring in it. Chemical reaction mechanism is one of the phenomena which should be counted on carefully. One can discover that not only one particular fully descriptive model, but those at several degrees of complexity necessarily exist in order to reproduce virtually realistic chemistry at reduced computational cost. For an ideal case, all chemical species expected to participate and relevant list of reactions should be appeared in the simulation. Turbulence effect on reaction rate and other scalar terms exists additionally in case of non-DNS turbulence modeling. Unfortunately, they would consume enormous computational resources if all

those are fully computed. Therefore it is easily derived that adequate assumptions for simplification of calculation relieves stiffness of the modeling in practice. For instance, while every chemical reaction has their characteristic time scale, it can often be assumed to be very short or long, which corresponds to infinitely fast chemistry or cold-flow respectively. Between these two, one can find a bunch of reaction model cases.

Type of fuel is one of the elements which determine the complexity of chemistry considered. In case of hydrogen fuel, number of participating species and reactions to be accounted for could be kept comparatively small. This advantage enabled many CFD researchers conduct simulations of hydrogen fueled system with low computational cost. In contrast, hydrocarbon fuels require much more calculations for up to hundreds of species and thousands of reactions at similar degree of accuracy. Up to date, most of hydrocarbon combustion models which can be combined with CFD have limited capability in detailed chemistry description. Cold-flow scramjet combustor simulation can be found massively. Several researches have demonstrated numerical analyses with infinitely fast chemistry on a scramjet combustor. Manna et al.[23] elaborated infinitely fast chemistry for liquid kerosene fueled scramjet combustor. In this research, no comparison with other modeling has been done. Meanwhile, Emory et al.[24] tried to use irreversible and infinitely fast chemistry model for comparison with tabulated chemistry of hydrogen fuel. Like these, comparison of reaction mechanisms for hydrocarbon fuel would be useful for further investigation of finite chemistry or other possible accurate modeling.

These basic modelings given above are lack of capability of predicting ignition characteristics and tracing intermediate products, especially trace species. Reduced reaction mechanisms which have limited species and reactions for low cost can be suggested

as a good alternative for a scramjet combustor numerical analysis. Jones-Lindstedt[25] and Li-Williams[26] have been chosen on account of their beneficial features.

In this chapter, four distinct reaction models are compared. Differences in their results such as shock intensity, mixing, flow and concentration are represented. These results would be valuable for proper approach to finite rate chemical kinetics and turbulent reaction rate which are closer to the exact solution and real nature.

3.2 Numerical methods and configuration

3.2.1 Numerical method

An in-house CFD code named F-com is capable of scramjet combustor simulation. For the capability, this code should be equipped with features for supersonic, unsteady, reactive and viscous flow. The computational domain may be divided into several blocks for flexible geometry implementation and parallel calculation. This code is parallelized using Intel message passing interface(MPI) library.

Favre-averaged multi-species Navier-Stokes equation is discretized with finite difference method with general coordinate transformation. For stable simulation of a supersonic flow, which can be expressed by a system of hyperbolic equations, MUSCL with Fromm's scheme[21] is used for upwind extrapolation and AUSM^{+}-up[19] for approximate Riemann solver. Under ideal gas assumption, NASA thermobuild 9-coefficient polynomial fitting[27] was used for obtaining thermodynamic properties such as specific heat from gas temperature. Calculation of transport coefficients which are viscosity, diffusivity and conductivity is based upon kinetic theory[28]. Detailed theoretical explanation can be found in Chapter 2. The code implemented Smagorinsky and dynamic LES model.

3.2.2 Configuration

For direct comparison with previous experimental results, flow simulation domain has been set to be the identical shape and size with the wind tunnel test rig. Detailed geometry of computational flow domain is depicted in figure 1 with constant width of 30 mm. It has fuel injection hole at the center of bottom wall and 18 mm apart from cavity leading edge. Experimental high-enthalpy wind tunnel is consist of a couple of auxiliary parts such as convergent-divergent duct, isolator, long expanding downstream nozzle and vitiator. With removing all these parts, computational domain has been restricted to the vicinity of fuel injection hole and cavity flameholder for low cost. The grid is much finer near fuel injection hole, as shown in figure 3. It has nearly 3 million nodes in total. Coarse and fine grid have been compared in figure 4. Coarse grid can resolve only very large integral structure, while base and fine grid are capable of detailed eddies around fuel jet.

From fuel concentration and temperature distribution in vicinity of fuel injection hole in figure 5, 6 and 7, it can be confirmed that side effect of orthogonal grid to round injection hole is restrictive. They show almost round distribution with slightly indented center.

The main flow contains some water vapor to imitate vitiated air. Its total temperature ranges between 2000 K and 2200 K, while injected fuel total temperature is constrained to 400 K. Mach number of the main flow is 2.0 and the fuel injection is choked. Equivalence ratio is set to be 0.163 which succeeded ignition in experiment.

Dirichlet type boundary conditions have been assigned for inlet and fuel injection hole, and Neumann type for outlet and wall. All walls are adiabatic and given no-slip condition. Initial condition for all nodes is shared from inlet boundary conditions.

3.3   Fuel combustion model

Methane has been chosen as the fuel concerned in this research. Although hydrocarbon fuels have several limitations in the aspect of vehicle operation when it is compared with hydrogen, they could be beneficial because hydrogen requires cryogenic condition to carry. In this point of view, there are better fuels such as kerosene which are widely used in experimental researches[29] [30]. Methane could be a good bridgehead for numerical analysis of hydrocarbon fueled engine, however, due to the fact that it is one of the simplest hydrocarbon and produced easily during fuel thermal cracking of heavier hydrocarbons.

Throughout chemical reaction, one kind of species would change into another kind of species. Chemical reaction consequently changes thermodynamic properties such as sensible energy, specific heat, temperature, pressure, density and transport coefficients. The fluid flow and transport phenomena are highly coupled with chemical reaction characteristics. Chemical kinetics is a key factor for analysis of combustion occurring in the engine. Controlling combustion in the engine is time-critical because of extremely short residence time, and more precise chemical kinetics is crucial for reliable research.

Even the simplest hydrocarbon requires hundreds of reactions to be exactly reproduced at any conditions such as pressure, temperature and equivalence ratio which is impractical in heterogeneous 3-dimensional reactor. This limitation leads to need for simpler models which can produce acceptably accurate results by calculation of rate of reaction at appropriate conditions and for specific objects.

3.3.1   Frozen chemistry and one-step fast chemistry

At first, one may regard a situation in which chemical time scale is much larger than flow time scale. This is equivalent to absence of chemical reaction. Since the flow in scramjet combustor is extremely fast, This can be a reference modeling for when the chemical reaction is too slow and effect of combustion is almost negligible. The result obtained with this modeling can be directly compared with experimental result from which is obtained with noble gases. In this modeling, all reaction rate term $\dot{\omega}$ is constrained to be zero.

While there is one extreme case of ratio between chemical and flow time scale, there would be a counterpart, which is one-step infinitely fast chemistry. This model assumes that all reactants instantly turns into final products, which are H_2O and CO_2 in this case. In practice this model hardly coincide with actual phenomenon in case of this fast-flow machine. However it can be thought to be an extreme of possible combustion mode occurred in a scramjet engine. In this modeling, chemical reaction takes place through only one overall step of oxidation of the fuel
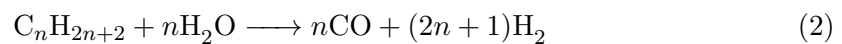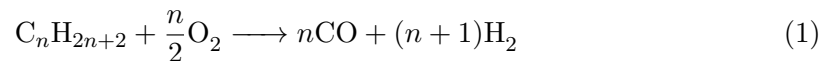
$$CH_4 + 2\,O_2 \longrightarrow CO_2 + 2\,H_2O.$$
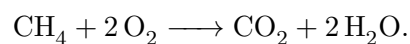
This modeling can be thought to be the situation of having infinitely fast reaction rate or similarly that all reactants are consumed within convectional time scale.

These two modeling does not require calculation of reaction rate. Therefore interaction with turbulence modeling is trivially unnecessary.

3.3.2 Jones-Lindstedt and Li-Williams model

The phenomena to be determined in combustion of methane are temperature rise by thermal energy release, change in the gas components and consequentially how the flow changes, or ignition delay time and flammability of the mixture. Appropriate models which are intended to these objectives would be useful for reproducing these phenomena in scramjet combustor simulation.
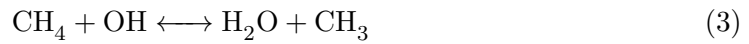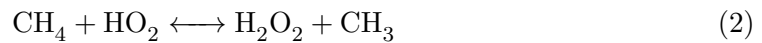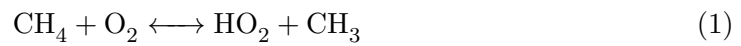
Jones and Lindstedt[25] suggested a reaction model that can calculate combustion of alkane C1-C4 fuels. This model is capable of both premixed and diffusion combustion regime. Objective of this model is to describe flame features such as flame speed, flame thickness and species profile, especially H_2 and CO with elimination of radicals and algebraically simple rate expressions. The authors expects that this model can be used for the case where detailed chemistry is computationally excessively costy or precise detailed chemistry is unavailable. The four-step reaction mechanism is

$$C_nH_{2n+2} + \frac{n}{2}O_2 \longrightarrow nCO + (n+1)H_2 \tag{1}$$

$$C_nH_{2n+2} + nH_2O \longrightarrow nCO + (2n+1)H_2 \tag{2}$$

$$H_2 + \frac{1}{2}O_2 \longleftrightarrow H_2O \tag{3}$$

$$CO + H_2O \longleftrightarrow CO_2 + H_2 \tag{4}$$

and $n = 1$ for methane.

Li and Williams[26] also suggested a reaction model. Contrast to the former, this model is derived with intention to capture features of methane ignition, rather than steady combustion. That is, the most important objective of this model is to

predict autoignition time, or in other words ignition delay time, of premixed methane-air mixture. This model has several variations with respect to their complexity, of which starts from a detailed base mechanism, and develops into further simplified versions with limiting assumptions. In this thesis, 9-step short mechanism has been used. Up to this short version, most of the flame ignition characteristics can be captured, and can perform moderate calculation cost. The reaction mechanism is

$$CH_4 + O_2 \longleftrightarrow HO_2 + CH_3 \tag{1}$$

$$CH_4 + HO_2 \longleftrightarrow H_2O_2 + CH_3 \tag{2}$$

$$CH_4 + OH \longleftrightarrow H_2O + CH_3 \tag{3}$$

$$CH_3 + O_2 \longleftrightarrow CH_2O + OH \tag{4}$$

$$CH_2O + OH \longleftrightarrow CHO + H_2O \tag{5}$$

$$CHO + O_2 \longleftrightarrow CO + HO_2 \tag{6}$$

$$CHO + M \longleftrightarrow CO + H + M \tag{7}$$

$$H + O_2 + M \longleftrightarrow HO_2 + M \tag{8}$$

$$H_2O_2 + M \longleftrightarrow 2\,OH + M \tag{9}$$

Details for these reaction models such as appropriate range, participating species, chemical formulas and their coefficients are given in 2 and 3. This model has been used in Bibrzycki and Poinsot[31]'s research with minor modification.

TABLE 2: Jones-Lindstedt hydrocarbon combustion global reaction schemes; concentration dependency and reaction rate constants. $k^f = AT^b e^{\frac{-E}{RT}}$.
(Units kg, m, s, kmol, cal, K)

Reaction	Reaction rate	A		b	E
(1)	$r^f = k^f[CH_4][O_2]$	0.44	$\times 10^{12}$	0.0	30 000
(2)	$r^f = k^f[CH_4][H_2O]$	0.30	$\times 10^{9}$	0.0	30 000
(3)	$r^f = k^f[H_2]^{\frac{1}{4}}[O_2]^{\frac{3}{2}}$	0.68	$\times 10^{16}$	-1.0	40 000
(4)	$r^f = k^f[CO][H_2O]$	0.275	$\times 10^{10}$	0.0	20 000

TABLE 3: Li-Williams methane ignition reduced reaction model
(Units cm, s, K, kJ, mol)

Reaction	A	b	E
(1)	3.98×10^{13}	0.00	238.0
(2)	9.04×10^{12}	0.00	103.1
(3)	1.60×10^{7}	1.83	11.6
(4)	3.30×10^{11}	0.00	37.4
(5)	3.90×10^{10}	0.89	1.7
(6)	3.00×10^{12}	0.00	0.0
(7)	1.86×10^{17}	-1.00	71.1
(8)	6.76×10^{19}	-1.40	0.0
(9)	1.20×10^{17}	0.00	190.4

Peters[32] and Bilger et al.[33] also suggested another good methane combustion models, which are hard to be used for this research because the case investigated is not steady and contains no radicals at startup.

When these two models are applied exactly, it is required to solve ordinary differential equation with respect to time. However, since each time step is sufficiently short for predominent cases, the rate of reaction is assumed to be constant. When if this comes to large error, the solution was obtained with forward Euler method. Also, if stiffness problem arises due to non-integer reaction order which can be found in Jones-Lindstedt model, the reaction is regarded as infinitely fast chemistry.

3.4 Differences due to combustion modeling

Combination of fluid-flow CFD code and each 4 combustion model produced their 4 results. The conditions between each combustion model cases are different. For frozen and fast chemistry cases, total temperature of the main flow is 2000 K, that of fuel injection is 500 K and pressure is 120 kPa. For Jones-Lindstedt and Li-Williams cases, total temperature of main flow is 2200 K, that of fuel injection is 400 K and pressure is 60 kPa.

All simulations have been run for physical time of more than 200 µs, which is enough time for injected fuel to reach outlet of the combustor. Those transient results have been time-averaged during $t = 100$µs and $t = 200$µs in order to attenuate temporal fluctuation and enable focusing on the differences of tendency.

Numerical Schlieren images in Figure 8 clearly reveal bow shock induced by fuel injection and following mixing layer development. Slightly modified angle of bow shock between cases sharing the same boundary conditions implies impact of combustion case selection. Because of different momentum ratio between main flow and the injection, mixing layer of Jones-Lindstedt and Li-Williams cases is more distinct.

The formation of the shock can also be confirmed by pressure distribution. Pressure on the upper wall along with flow direction is frequently given in experiments for simple measurement, and it can be compared with numerical results shown in figure 9. On frozen/fast chemistry pair and Jones-Lindstedt/Li-Williams pair compared, the peak of wall pressure seems to come closer and the magnitude is intensified for fast chemistry and Jones-Lindstedt cases. It is expected that higher peaks are resultant of active and vigorous combustion. This can be supported by pressure distribution on xy plane shown

in figure 10 which contains more detailed information. As expected, those modified wall pressure peaks are originated from strengthened shock at injection impingement.

In previous studies[34][35], pressure rise in the vicinity of fuel injector is pretty high compared to the present result. Usually, with higher equivalence ratio comes higher pressure peak. This implicitly indicates that overfuelling results in thermal choking, regardless of chemical reaction. or mixing is not fully executed.

On the same plane, examining distribution of temperature and participating species can broaden our understanding on behavior of the combustor. Figure 11 discloses the fact that substantial temperature increase exists in fast chemistry and Jones-Lindstedt cases while Li-Williams marginally raises it. From this figure it is clear that combustion behavior between Jones-Lindstedt and Li-Williams is quite different. This difference is confirmed in the figure 12, 13 and 14. While methane takes part in all cases, carbon dioxide belongs to fast chemistry and Jones-Lindstedt cases, and OH appears in only Li-Williams case. Experimental high-speed camera snapshot in figure 15 could be compared with these numerical results. At early ignition stage, existence of autoignition is observed, while there is no developed flame established. At developing flame stage, light emitting region expands upstream up to cavity leading edge. At Developed flame stage, combustion is maintained by cavity flame holder. This process requires approximately a few milliseconds.

From the distribution of methane, it is shown that mixing of the fuel with main flow is achieved above cavity flameholder. for fast reaction models the fuel is consumed at the end of the cavity, while the other cases the fuel persists to the end. Since simulated period is comparatively short, most mixing is triggered by fuel injection rather than by shear layer formed by the cavity. Carbon dioxide distribution of the Jones-Lindstedt case is thought to be a more realistic result when compared to fast chemistry case.

While fast chemistry case represents mixed-is-burned situation, from Jones-Lindstedt case result it is confirmed that accumulation of combustion product commences within the cavity. OH radical distribution also supports this phenomenon.

The reason for absence of vigorous combustion in case of Li-Williams case can be explained from experimental result. During ignition process, accumulation of radicals in the vicinity of cavity trailing edgy and downstream boundary layer after cavity proceeds development of the flame which can be confirmed from figure 15. Distribution of OH radical coincides quite well with the region where autoignition exists in experiment. Therefore, reproduction of ignition process by Li-Williams model is thought to be achieved successfully.

Specific and detailed argument on relation between combustion model and combustion behavior, mixing and combustion efficiency have been evaluated quantitatively. Since chemical reactions of hydrocarbon species take place, the definition of mixing efficiency should be calculated by distribution of elements, not that of substances. The definition of mixing efficiency is given as

$$\eta_{mix} = \frac{\int_A \alpha \rho u Y_{fuel} \mathrm{d}A}{\int_A \rho u Y_{fuel} \mathrm{d}A}$$

where

$$\alpha = \begin{cases} {}^1/_\phi & \text{if } \phi \geq 1 \\\\ 1 & \text{if } \phi < 1 \end{cases}$$

$$\phi = \frac{X_{O,st}}{X_O} = \frac{2X_C + \frac{1}{2}X_H}{X_O}$$

$$X_s = \sum_{i \ni s} n_i \frac{w_i}{M_i}.$$

$$Y_{fuel} = Y_C + Y_H$$

This definition for hydrocarbon combustion is an extended version from Gruber et al.[6] formula which was applicable to hydrogen fuel. And the definition of combustion efficiency is presented as

$$\eta_{comb} = 1 - \frac{\int_A \rho u Y_{CH_4} \mathrm{d}A}{\int_A \rho u Y_C \mathrm{d}A}$$
$$= 1 - \frac{\int_A \rho u Y_{CH_4} \mathrm{d}A}{\int_A \rho u (Y_{CH_4} + Y_{CH_3} + Y_{CO} + Y_{CO_2}) \mathrm{d}A}.$$

Those efficiencies are shown in figure 16 and 17.

From mixing efficiency, any obvious relation between reaction model and mixing is not found. Comparison between frozen and fast chemistry is apparently opposite to that between Jones-Lindstedt and Li-Williams. Since mixing occurs through vorticity generation, velocity difference against fluid flows, orthogonal gradient of pressure and density and interaction between injection and shear layer are to be taken into account in order to clarify relation of mixing and combustion modeling. Although few amount of radicals were measured from Li-Williams model simulation, overall combustion efficiency is virtually zero. This is more realistic than any other modelings, because this ignition behavior is found in many previous experimental results. Combining mixing and combustion efficiency, even for mixed-is-burnt modeling, their absolute value is quite different. This is thought to be rooted in the definition of the efficiencies.

Additionally, in figure 10, it is observable that well-developed mixing layer is entrained into the cavity and collides with its backwall and conforms high-pressure region in the vicinity of cavity downstream edge.

3.5　Conclusion

Simulation of two reduced chemical modelings along with simpler and more extreme frozen and infinitely fast chemistry modeling have been performed in hydrocarbon fueled cavity flame holder assisted scramjet combustor and their results are compared. Information from formation of bow shock induced by fuel injection, distribution of pressure, temperature, concentration and Mixing and flow characteristics were notably affected by each combustion modeling. From the results above, Jones-Lindstedt modeling permitted active combustion. This modeling effectively removed spurious phenomena of fast chemistry, while enough for examining effect of combustion on the flow and operation of engine combustor. On the other hand, from Li-Williams modeling, consequences which are thought to be arose in the initial stage of ignition are quite similarly represented. Consequently, Li-Williams modeling would be a good candidate for simulation intended for reproducing ignition sequences. Meanwhile, Jones-Lindstedt would be an alternative method when one eager to observe combustion characteristics without addressing ignition problems. This investigation would be a good milestone in quantitative verification of chemical reaction modelings for hydrocarbon fueled scramjet engines.
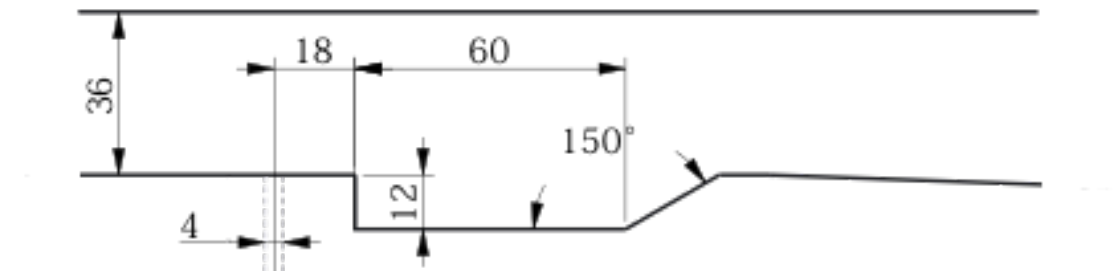
FIGURE 1: A schematic of scramjet engine combustor
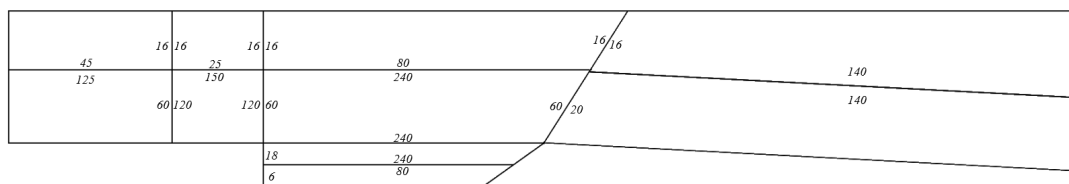
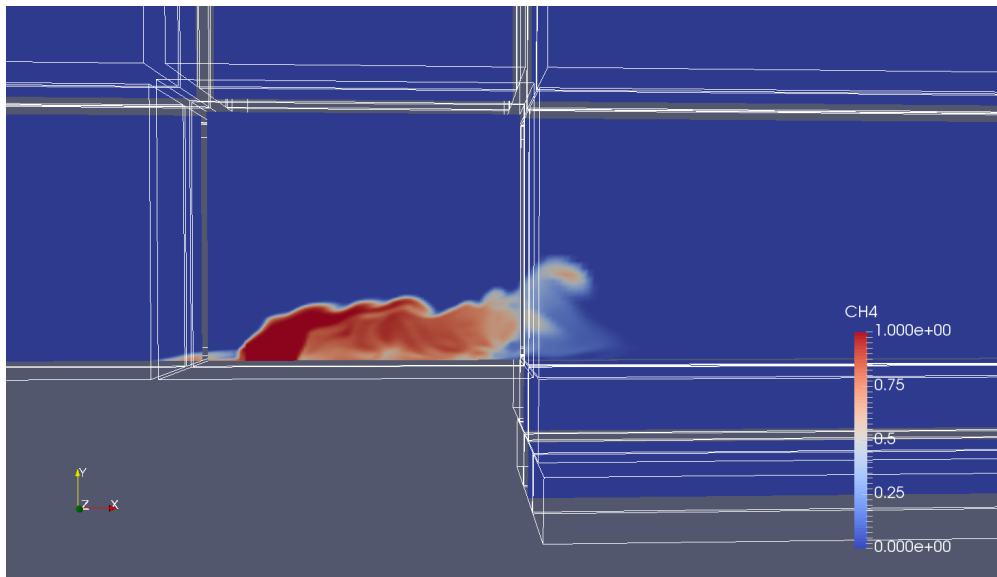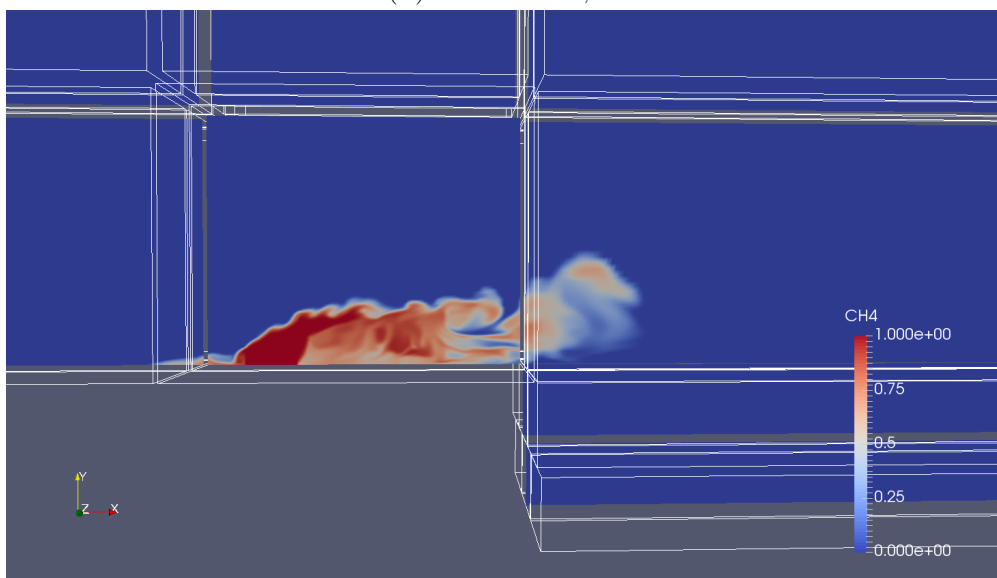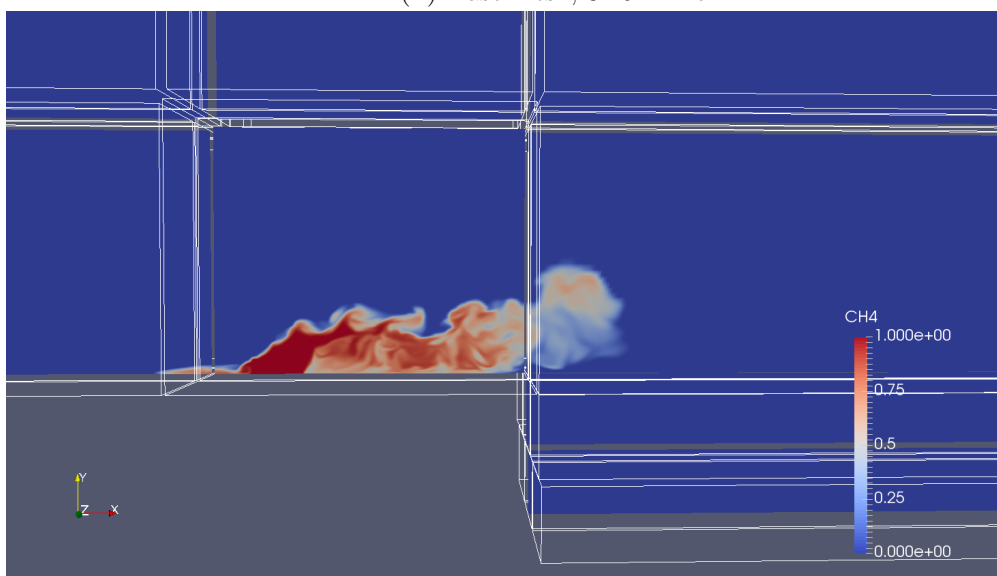FIGURE 2: Grid configuration layout for computational domain
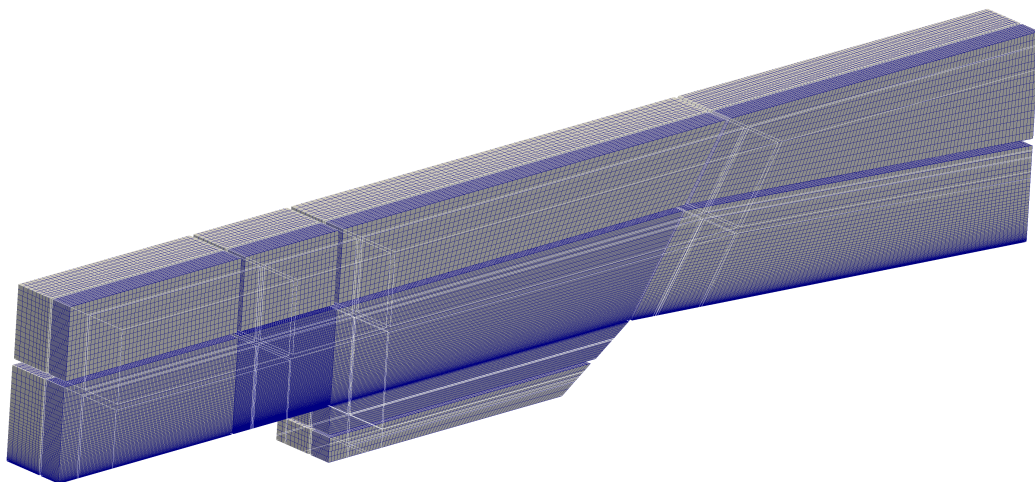
FIGURE 3: Isometric view of numerical domain grid. Half of grid blocks are explicitly shown.

(A) Coarse mesh; 1.62 million

(B) Base mesh; 3.16 million

(C) Fine mesh; 6.17 million

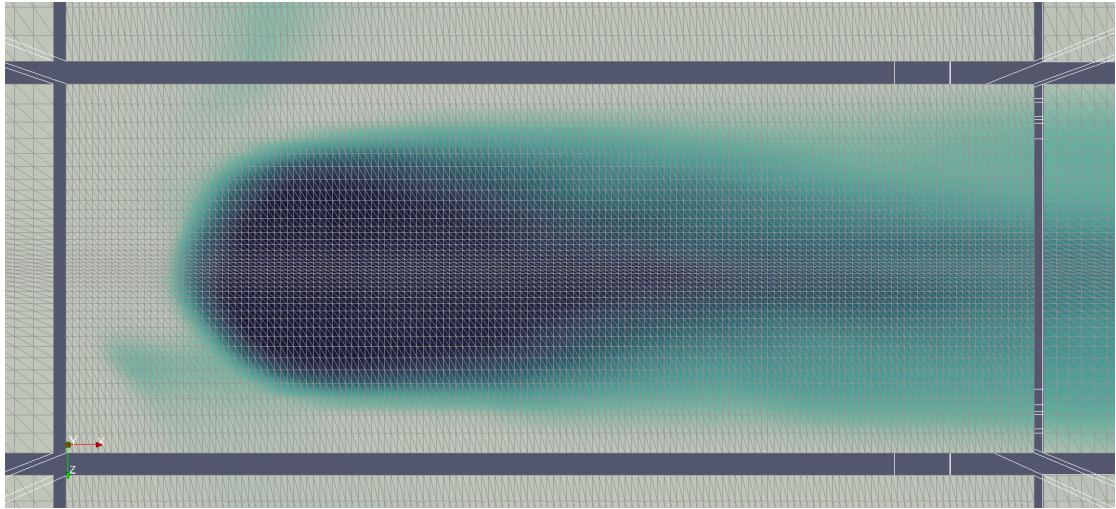FIGURE 4: Methane concentration near injection hole

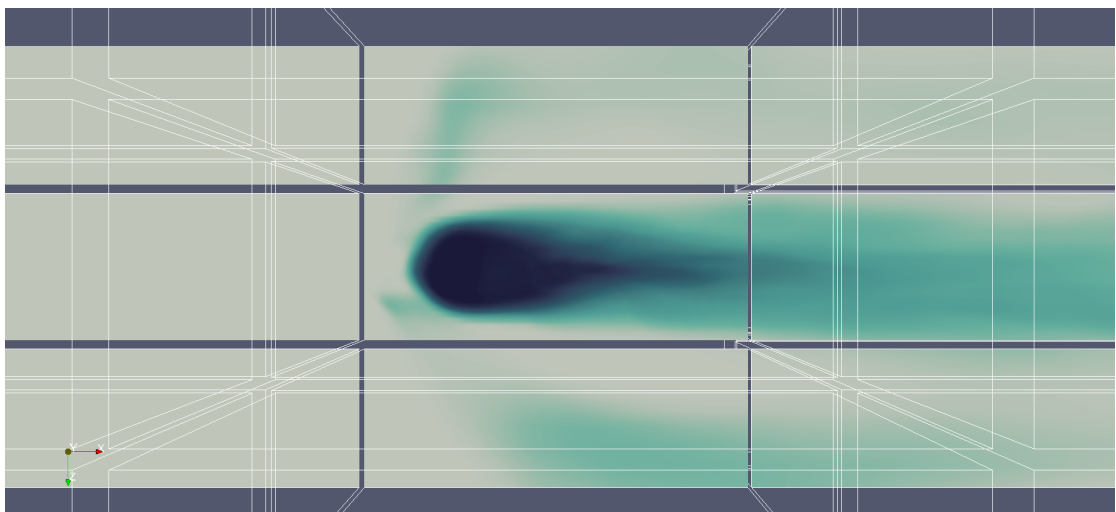FIGURE 5: Methane concentration in small vicinity of injection hole on horizontal plane $z = 0.1\,\mathrm{mm}$

FIGURE 6: Methane concentration in large vicinity of injection hole on horizontal plane $z = 0.1\,\mathrm{mm}$
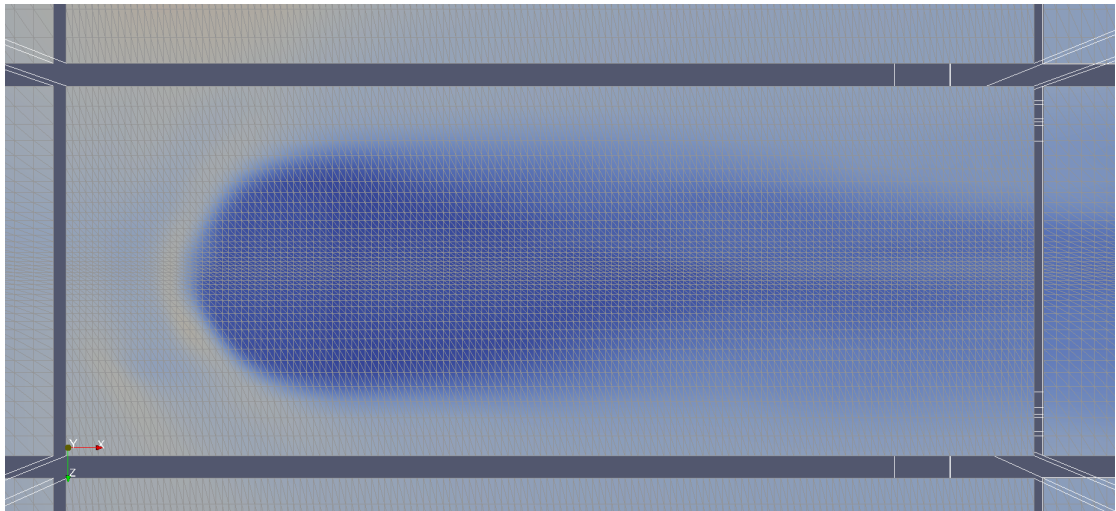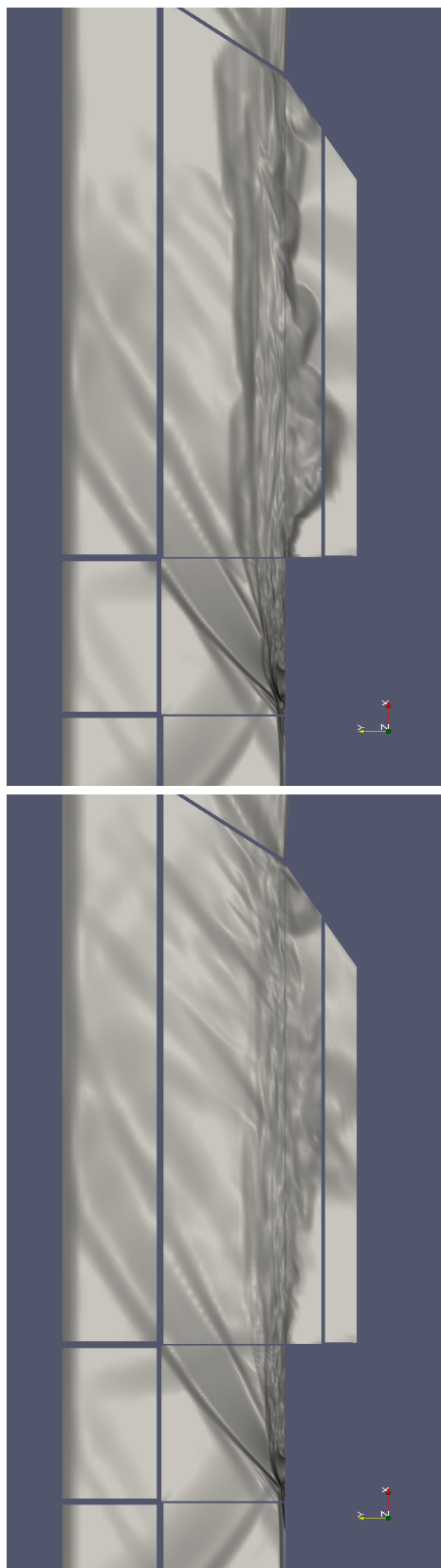
FIGURE 7: Temperature distribution in vicinity of injection hole on horizontal plane $z = 0.1\,\mathrm{mm}$

(A) Frozen

(B) Infinitely fast chemistry
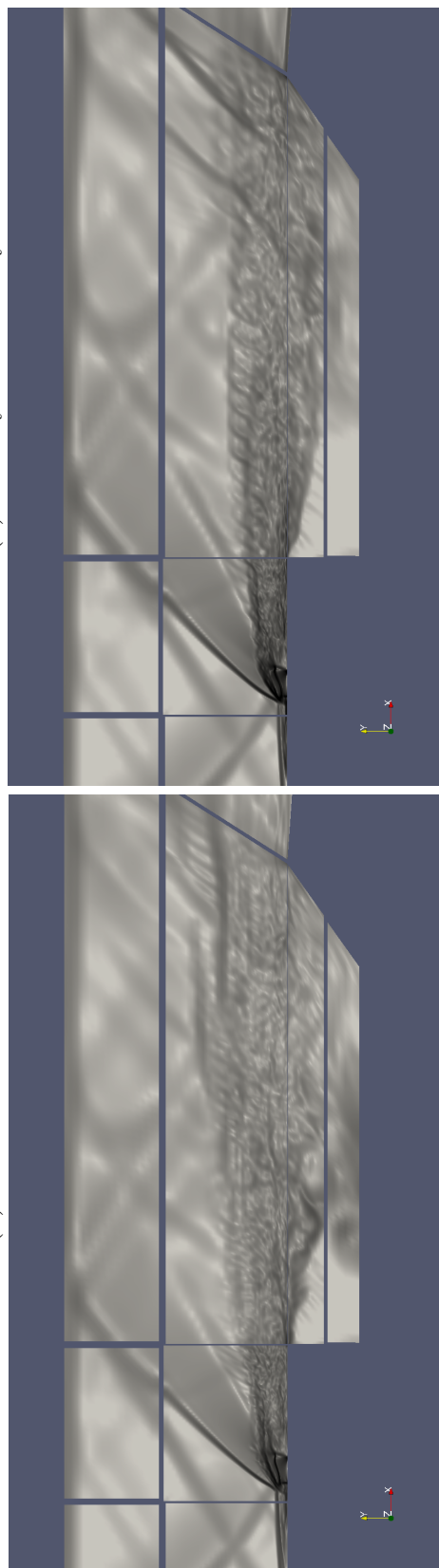
(C) Jones-Lindstedt

(D) Li-Williams

FIGURE 8: Numerical Schlieren images of each combustion model results.
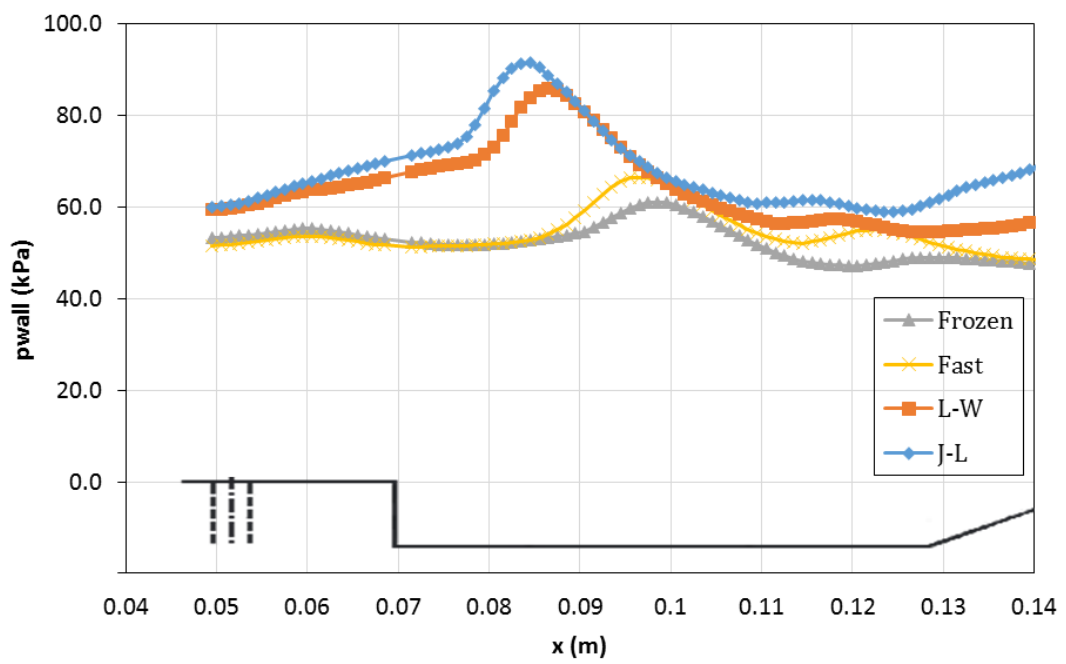The images show density gradient magnitude on xy plane passing the center of combustor.

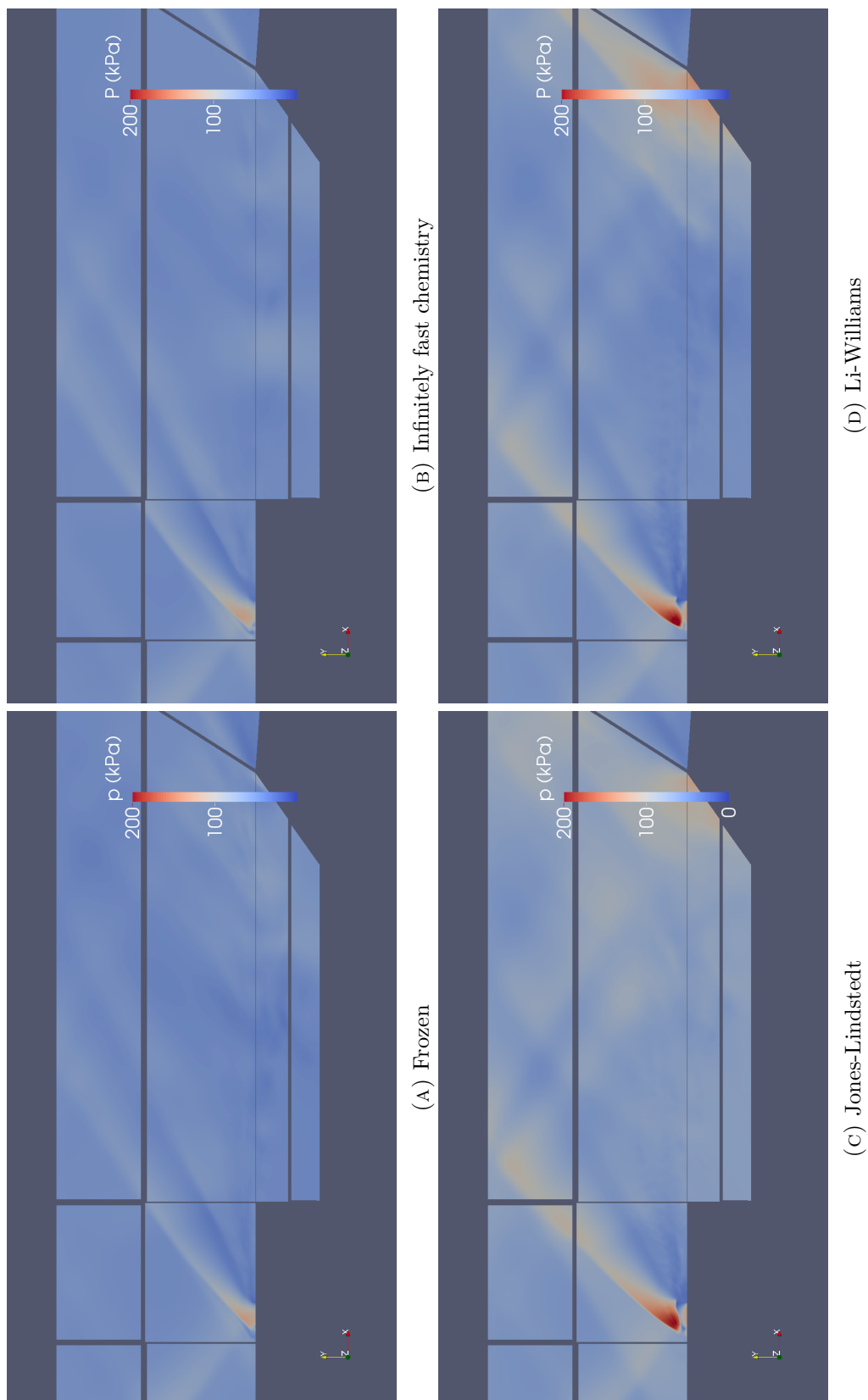FIGURE 9: Wall pressure distribution on the upper wall center with respect to various chemical modeling cases
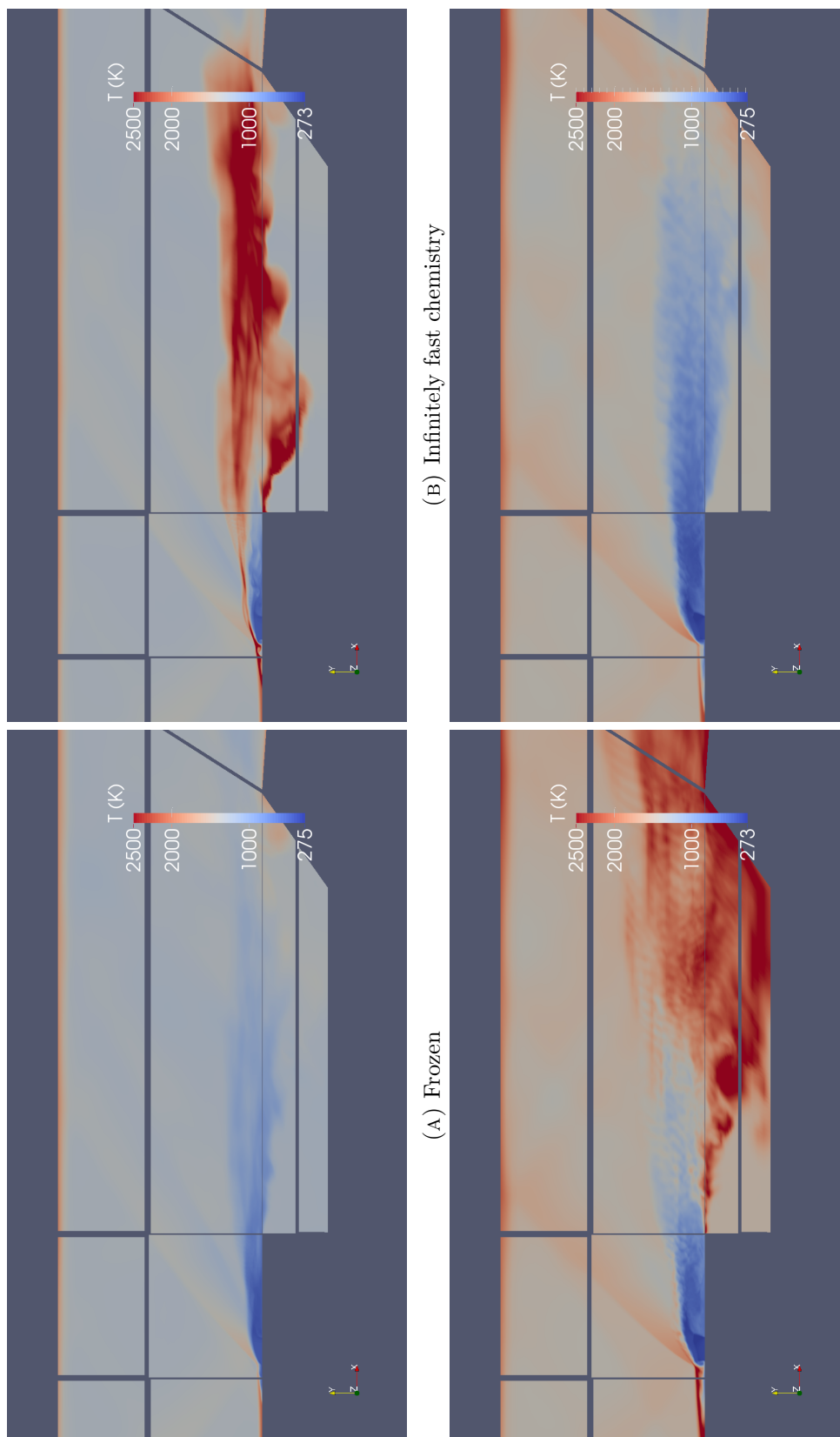
(A) Frozen

(B) Infinitely fast chemistry

(C) Jones-Lindstedt

(D) Li-Williams

FIGURE 10: Pressure distribution of each combustion model results.
The images show static pressure on xy plane passing the center of combustor.

(A) Frozen

(B) Infinitely fast chemistry

(C) Jones-Lindstedt

(D) Li-Williams

FIGURE 11: Temperature distribution of each combustion model results.
The images show static temperature on xy plane passing the center of combustor.
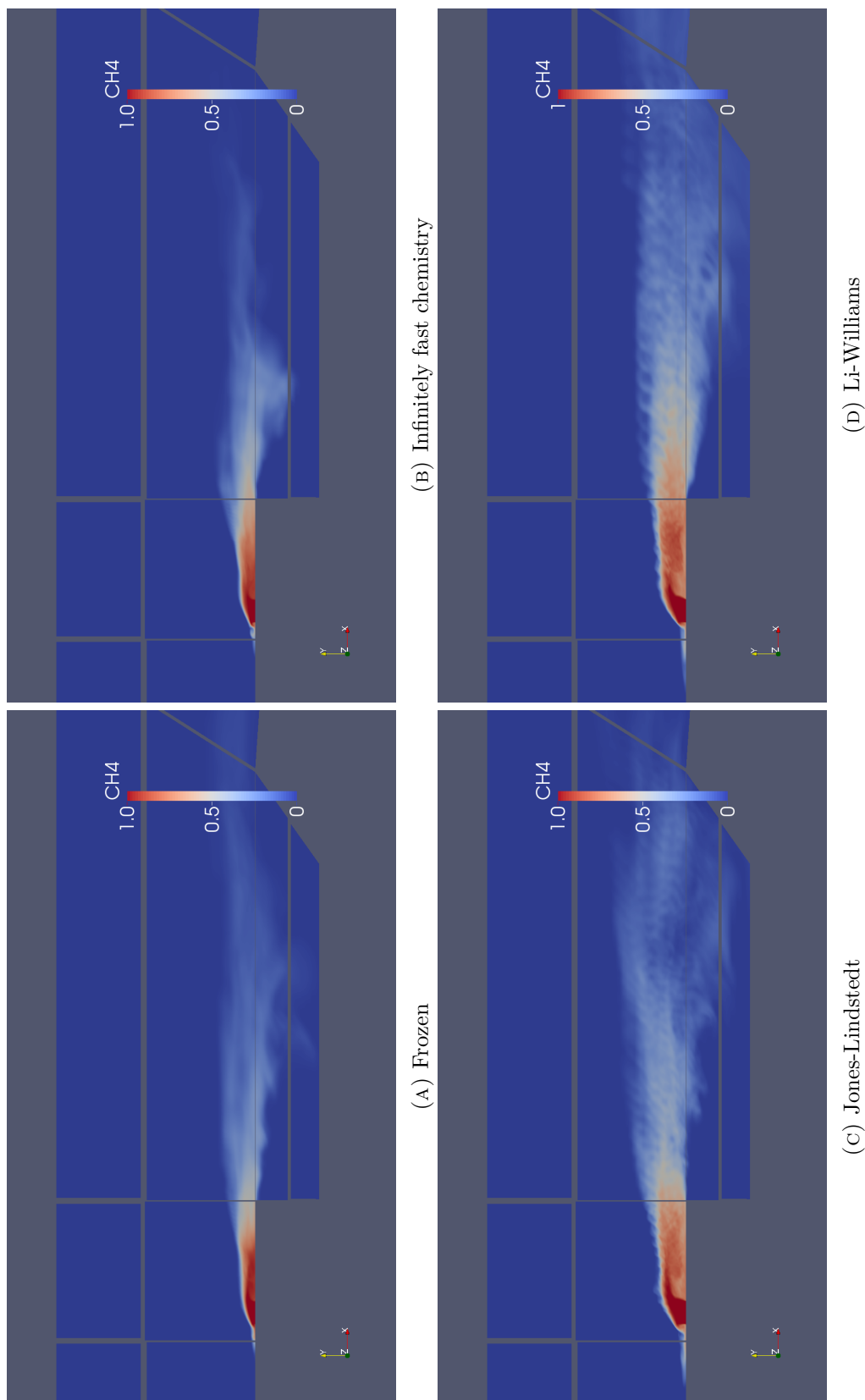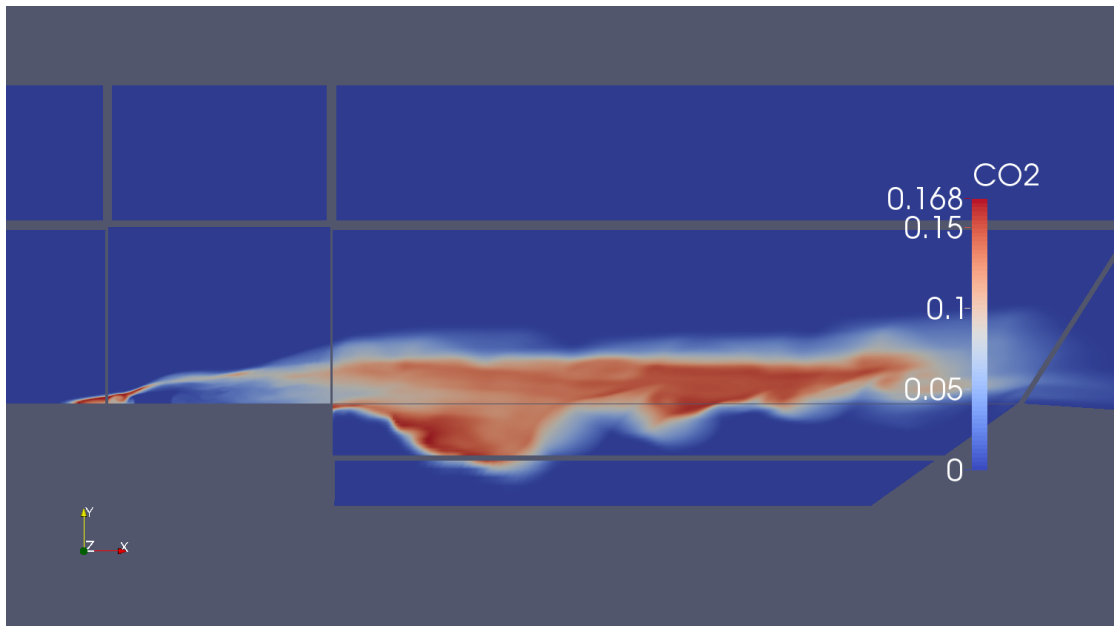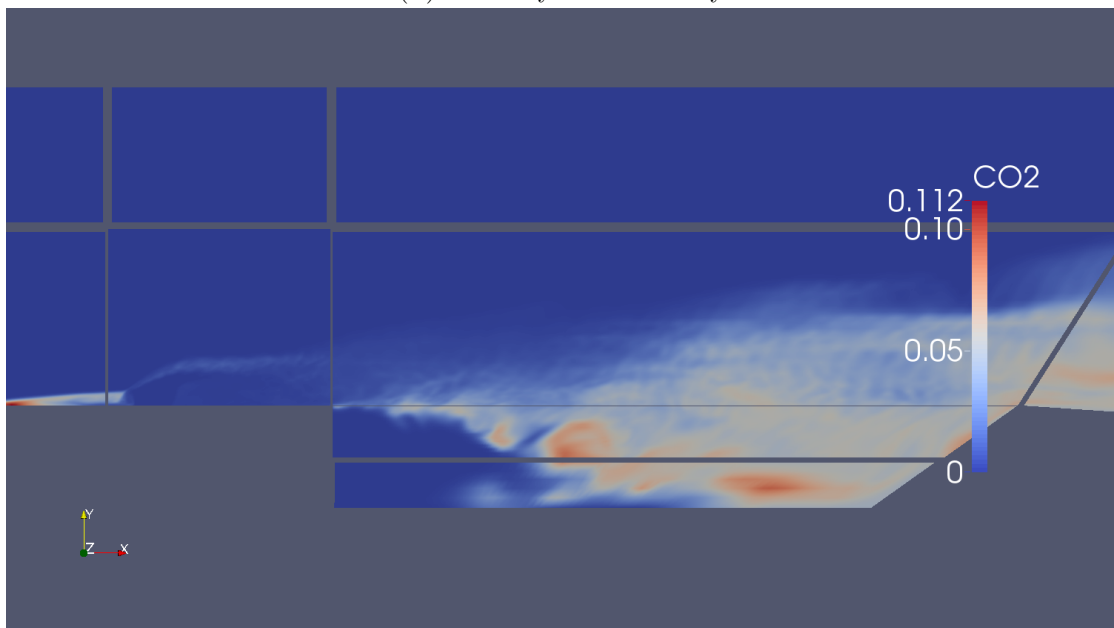
(A) Frozen

(B) Infinitely fast chemistry

(C) Jones-Lindstedt

(D) Li-Williams

FIGURE 12: Methane distribution of each combustion model results.
The images show mass fraction of CH_4 on xy plane passing the center of combustor.

(A) Infinitely fast chemistry

(B) Jones-Lindstedt

FIGURE 13: Carbon dioxide distribution of two combustion model results. The images show mass fraction of CO_2 on xy plane passing the center of combustor. CO_2 is not included as participating species in excluded combustion models.

FIGURE 14: Hydroxyl radical distribution of Li-Williams combustion model results. The images show mass fraction of OH on xy plane passing the center of combustor.
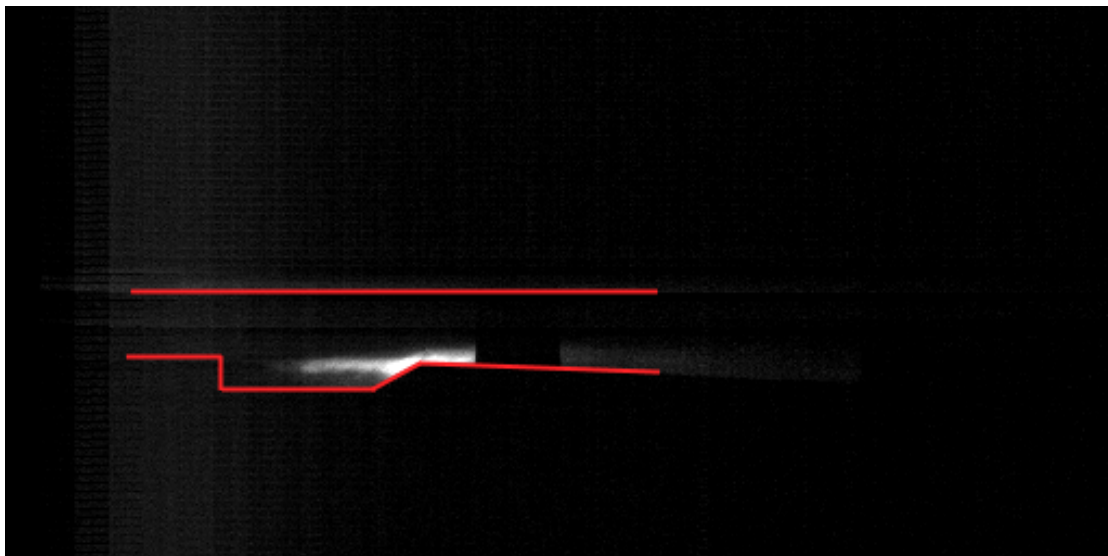
(A) Early ignition stage
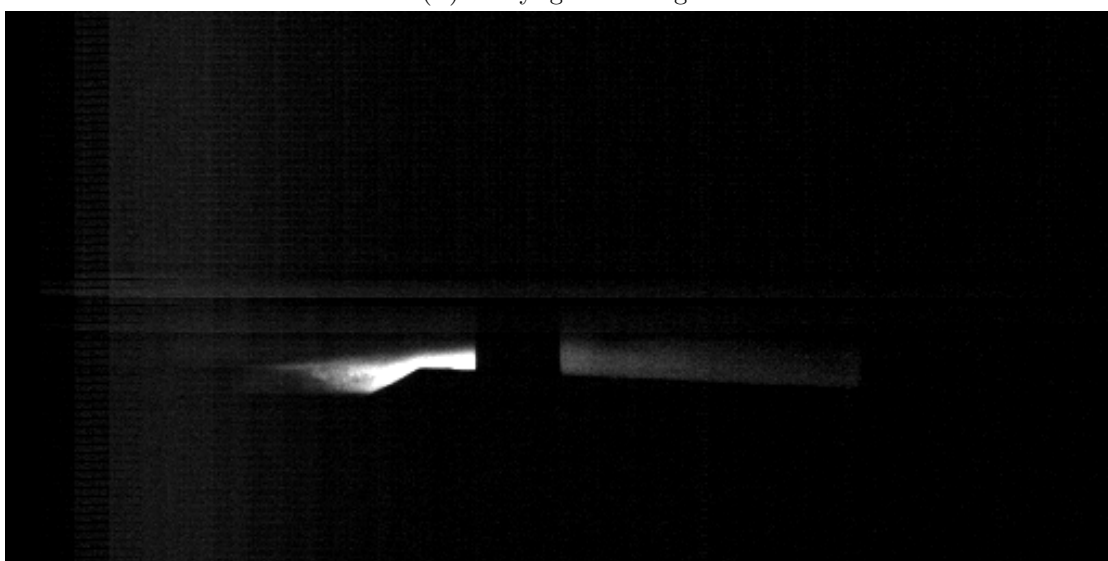
(B) Developing flame stage
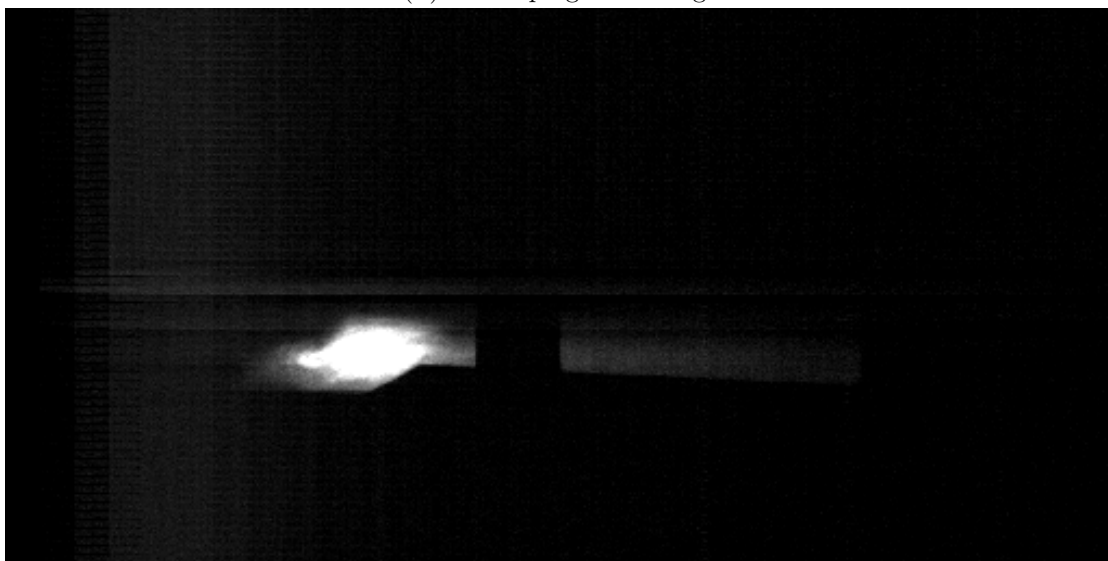
(C) Developed flame stage

FIGURE 15: Visual light snapshots of high-speed camera experiment at $\phi = 0.153$ and fuel consisted of 40 % C_2H_6, 60 % CH_4

FIGURE 16: Mixing efficiency of the fuel on yz plane along flow direction with respect to fuel combustion model
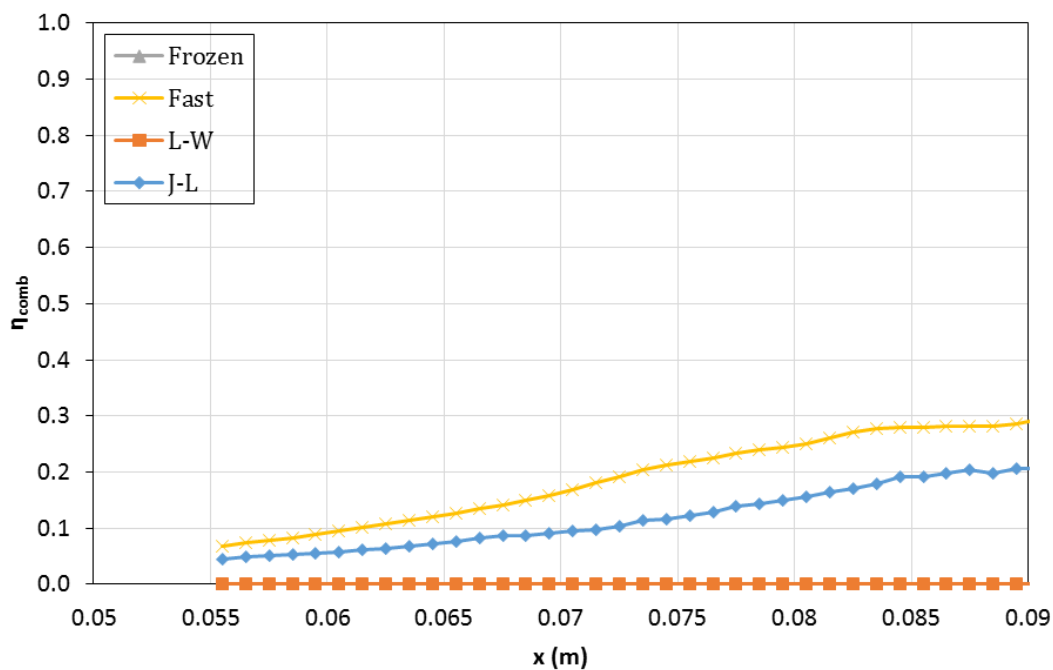
FIGURE 17: Combustion efficiency of the fuel on yz plane along flow direction with respect to fuel combustion model

Chapter 4

Effects of Fuel Heating on Supersonic Crossflow Behavior with Combustion

4.1   Introduction

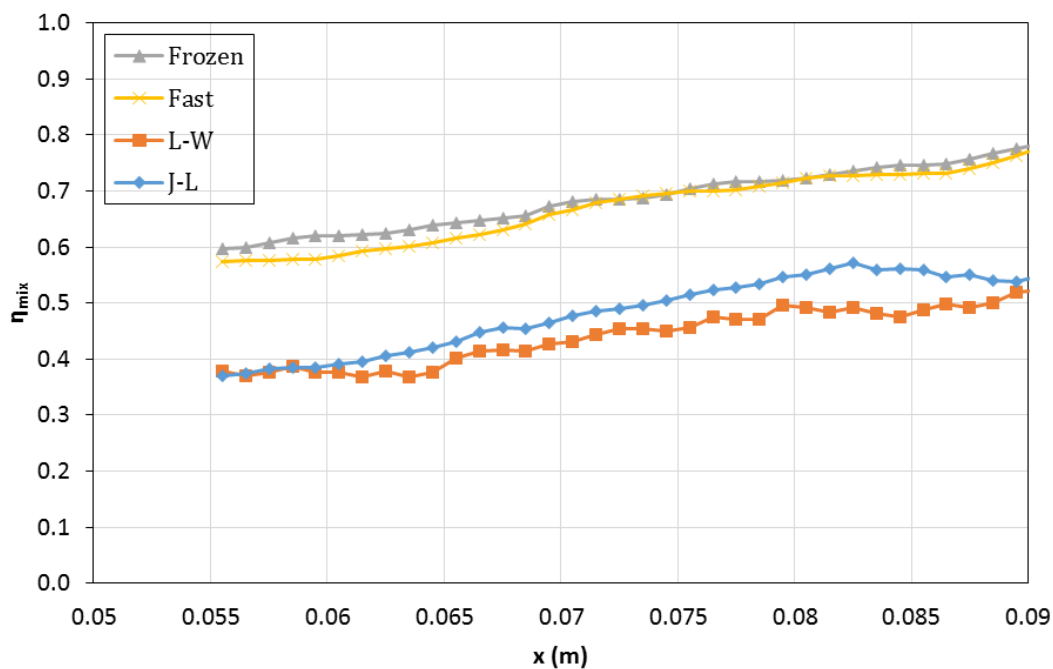From the advent of scramjet engine, despite of decades of development and enormous concern, still no practical vehicle with purpose has ever flown. That ignition, control and stabilization of combustion of injected fuel into super-fast air stream is tortuous can be attributed to the reason of development doldrum. For combustion stabilization and engine control, various fuel injection techniques and flame holding devices have been adopted to a scramjet combustor. Cavity/strut flame holder, air ramp, backward-facing step, ignition with electric/optic igniter, pilot flame and fuel injection configuration are several representative methods.

One may control scramjet engine combustion behavior effectively by adjusting the properties of fuel injection. The properties to be modified would be participating chemical species or their composition ratio of the fuel, injection position, intensity or orientation, and global equivalence ratio[2] [36] [37] [1]. Among them, transverse injection is quite strong method to control combustion behavior. the impact of the injection on combustor effectiveness can be both positive and negative. In general, it enhances mixing due to complex flow induced by bow shock wave and horseshoe vortex generation, while deteriorates main flow momentum due to blockage. Out of many aspects of fuel injection, momentum of the jet with respect to main flow is an important factor in mixing. Penetration of the fuel is mainly determined by the dynamic pressure ratio[38]. Meanwhile other factors may affect mixing in various mechanisms.

Heating of the fuel is often inevitable for hypersonic vehicles. This is due to the fact that hypersonic vehicles have limited cooling methods during its service. As the fuel cools engine component or surface of the vehicle, not only operability of the vehicle is extended, but also energy efficiency and controllability are improved by endothermic reaction of the fuel which changes its heavier hydrocarbons into lighter one. Here, too high fuel temperature leads to coke formation which hinders fuel supply system functionality.[39] This phenomenon mandates a limitation to the maximum fuel temperature.

Fuel temperature can be chosen as an attractive injection controlling factor. Wendt et al.[11] conducted an interesting experiment on effect of fuel stagnation temperature on mixing of supersonic flows. The researchers claimed that the important factor for mixing was vorticity generation by velocity difference. Even with higher temperature, if that results in reduced velocity difference, mixing efficiency is decreased, which is thought to be a valid argument. This result implies that higher temperature is not always a favorable factor for mixing, while higher total enthalpy typically enhances continuous

combustion controllability. However, this considered only longitudinal, parallel flow with respect to the main flow, and lacking in traversing case, which is important for scramjet combustor as well. When the two flows are parallel, Only velocity difference makes the par to be mixed. However, with transversing flows, it becomes quite complicated and other factors should be considered.

In this chapter, Behavior of supersonic methane fuel jet combustion with respect to fuel total temperature will be numerically investigated by revealing effects of dynamic pressure ratio change between fuel jet and air flow and fuel temperature change. Pressure distribution, penetration, mixing and combustion efficiency are analyzed to study factors that controls combustion in scramjet combustor.

4.2 Numerical method

Owing to the conclusion of chapter 3, methane has been chosen as a primary fuel and Jones-Lindstedt combustion modeling has been applied to the code. With this modeling, the solution is expected to be able to capture main features of combustion behaviors as well as supersonic crossflow. Also that the issue is not related with ignition characteristic was considered for selection of combustion model.

Chemical reaction kinetics and compressible fluid flow calculation could be conducted by a Fortran multi-threaded simulation code. Time-evolving solutions were obtained. For detailed information about the code, one can refer to section 3.2.1.

Those reaction rate expressions which is based on Arrhenius's formula form a system of ordinary differential equations. For lowering calculation cost, in most cases temporal derivative of concentration was assumed to be constant. That is, during one timestep, rate of reaction was evaluated just once. while this was fair enough for most

area of the domain, multi-timestep integration was performed where change of concentration exceeded certain amount of current concentration at a point. As a result, overall reaction rate is thought to be slightly overestimated, but it hardly affects analysis about mixing, which is a main objective of this research.

For consistent comparison with previous experimental results, flow domain has identical shape and size with the experimental test rig. Figure 1 shows a detailed geometry of flow region. Only combustor part which holds an injection hole and a cavity flame holder is considered in the simulation exclusively. The computational region has 30 mm width, and has a circle fuel injection hole at the center of bottom wall in front of cavity leading edge. The fuel is injected transversely into the freestream.

Since it is desirable to investigate effects of fuel heating, injected fuel total temperature has been chosen to be an independent variable, while momentum ratio between fuel injection and main flow has been altered for comparison. Equivalence ratio has been constrained to 0.163. This equivalence ratio lead to successful combustor operation in previous experiments. Main flow which comes in through inlet of the combustor is composed of pure air and water vapor at adjusted properties of atmosphere which can be a design point for a flight mission. Main flow total temperature is 2200 K, Mach number is 2.0 and static pressure is 52 kPa. Concentration of water vapor contained is determined as 14 % in volume to imitate vitiation effect of experiments. All walls are adiabatic. Zero-gradient Neumann boundary condition has been assigned to outlet area. Initial conditions in the domain are identical with inlet conditions. One exception is velocity of fluid in cavity flame holder which is set to be still.

Either dynamic pressure ratio of fuel injection or total temperature of fuel has been constrained to a certain value for the cases to be compared. For compensation of low dynamic pressure in low temperature cases, numerically inactive methane is augmented

to the fuel and that mixture is injected into main flow. The dynamic pressure ratio and total temperature of each case can be found on table 4. The highest fuel temperature has been chosen upon discussion from Huang et al.[39] which prevents coke formation. The flow is choked at the fuel injection outlet.

TABLE 4: Fuel injection conditions for penetration test. Equivalence ratio and Mach number have been constrained to 0.163 and unity for all cases, respectively.

Case	T_t (K)	T (K)	J	v (m/s)	$\dot{m}$ (g/s)	$w_{CH_4,inactive}$ %	p (kPa)
1	400.0	350.862	0.572	482.5	4.00	0.0	119.9809
2	400.0	350.862	0.635	482.5	4.44	9.9	133.1788
3	400.0	350.862	0.691	482.5	4.83	17.2	144.9369
4	400.0	350.862	0.743	482.5	5.20	23.0	155.7352
5	400.0	350.862	0.792	482.5	5.53	27.7	165.9335
6	500.0	447.0	0.792	535.4	4.98	19.7	171.6318
7	600.0	544.788	0.792	582.8	4.58	12.7	176.6065
8	700.0	643.0	0.792	626.4	4.26	6.1	180.3938
9	800.0	741.340	0.791	667.2	4.00	0.0	183.3461
10	600.0	544.788	0.691	582.8	4.00	0.0	154.2415

Unsteady continuity, Navier-Stokes, energy and chemical species balance equations has been solved simultaneously. Considering convergent time marching, the time interval was determined to keep Courant number lower than 0.3, which was also suitable for proper reaction kinetics calculation. At $t = 0$ s, fuel is about to be blown out from injection hole. For all cases the simulation reached more than 150 µs. The results which was time-averaged during last 50 µs are used for overall analysis and compared with instantaneous results.

4.3   Results and Discussion

In this section, Each cases are compared with relevant ones. The cases with pure methane injection, i.e. no augmentation of inactive methane, will be compared first, and then effects of dynamic pressure ratio and that of total temperature as an exclusive independent variable to each other will be contrasted with several parameters. These three comparison forms a triangle in figure 18.

4.3.1   Temperature, concentration and flow field representing combustion field at mid-plane

From flow field in figure 19, typical structure of supersonic transverse jet could be observed[38]. Barrel shock and Mach disk imply underexpanded injection flow and bow shock and recirculation zone are created by collision between air and fuel flow. Large vortices above cavity flame holder are also observed clearly. Figure 20 locates the region where strong vortices exist and enhance mixing. Along the fuel column, vortices works as a main mechanism of fuel mixing.

Temperature and concentration of active methane on mid-plane at $z = 15\,\mathrm{mm}$ are provided in figure 21 and 22 for instantaneous results and figure 23 and 24 for time-averaged results. Representative cases were selected so that differences could stand out perspicuously. Fuel temperature condition difference can be identified by color near injection hole. Red regions which has temperature higher than $2000\,\mathrm{K}$ indicates presence of combustion. For inactive methane mixed case 5, concentration is lower than unity. From those results, it could be identified that flow in the cavity is still not in equilibrium while flow over the cavity shows its characteristics distinguished by given conditions.

4.3.2 Wall pressure distribution and numerical Schlieren image

Figure 25, 26 and 27 shows static pressure distribution on the middle line of the combustor upper wall. Center of fuel injection hole is at $x = 0.052$ m and the cavity flame holder starts at $x = 0.07$ m. Figure 25 compares pure active methane cases. Peaks near $x = 0.08$ m represents bow shock created by fuel injection. The bow shock can be seen on a numerical Schlieren image in figure 28. Figure 26 compares exclusive deviation of dynamic pressure ratio cases. The dynamic pressure ratio and the pressure peak value are proportional. The result explains that stronger bow shock forms at higher dynamic pressure ratio, which leads to greater loss from irreversible process. Figure 27 compares exclusive deviation of total temperature cases. No distinct deviation can be found among the cases, suggesting that intensity of bow shock is not related to the fuel temperature.

After $x = 0.11$ m the pressure becomes quite unstable. Those pressure patterns originate from the vortices and combustion of injected fuel and surrounding air mixture, which can be confirmed from figure 28. The patterns imply unsteady nature of flow in vicinity of the mixing zone of the fuel and air. They are irrelevant to either dynamic pressure ratio and total temperature.

4.3.3 Penetration of fuel jet

Penetration can be analyzed quantitatively in various ways. Smith and Mungal[40] has chosen highest peak of contour obtained from ensemble-averaged PLIF image. This would correspond to pathline of the fuel injection. Gruber et al.[1] determined penetration depth as the position of which fuel concentration is 10 %. Similarly, Ben-Yakar et al.[2] suggested 1 % concentration as criterion. Those are suitable for experimental research since they can be obtained easily. In contrast, for numerical research, centerline

of the fuel jet can be calculated readily. In this research, Averaged height of the fuel is defined as a parameter for penetration and diffusion of the fuel jet. Definition of the parameter is stated below.

$$\bar{y} = \frac{\int_A y \rho u Y_{\mathrm{C}} \mathrm{d}A}{\int_A \rho u Y_{\mathrm{C}} \mathrm{d}A}$$

Pure active methane cases are compared in figure 29. By increasing total temperature of fuel, penetration became stronger. Above the injection hole, there is a peak, and the average height slightly decrease. This may be attributed to mixing process which is stronger below the fuel jet. Increased penetration rate at downstream in $T_t = 600\,\mathrm{K}$ case is notable.

Constant fuel temperature and varying dynamic pressure ratio cases are represented in figure 30. Near the injection hole, the penetration is dominantly dependent upon dynamic pressure ratio as concluded by Billig and Lasky[38]. As the jet flows to the downstream, however, difference in height is diminishing. This also can be regarded as behavior of mixing rather than convective penetration.

Also constant dynamic pressure ratio and varying fuel temperature cases are represented in figure 31. Near upstream region, there is no difference in average height, which means the temperature and consequently mass flow rate / density / velocity does not affects penetration noticeably. The behavior of downstream indicates that the average heights become slightly different in order of increasing temperature.

4.3.4 Mixing and combustion efficiency

Fuel-air mixing process can be divided into 3 stages. At the first stage, the fuel is injected into the main flow. This is a bulk flow of the fuel, and its effect on mixing can

be addressed by jet penetration analysis. The most important parameter at this stage is penetration characteristics. At the downstream of bulk motion flow, the fuel in the jet column is entrained into the surrounding air by vortices. Those vortices are to be created and intensified mainly due to turbulence, also including effect of jet impingement, shock wave interaction and boundary layer. As the lumps of fuel and air are mixed off into smaller scales, the final step would be molecular diffusion which is necessarily followed by an inception of chemical reaction chains. Definitions of mixing and combustion efficiency are the same with those of 3.

Combustion efficiencies among pure active methane cases are compared in figure 32. $T_t = 800\,\text{K}$ case exhibits better efficiency at first, but $T_t = 600\,\text{K}$ case overtakes it at downstream. The reason for this crossover would be found by investigating other cases. In figure 33 and where constant fuel temperature and varying dynamic pressure ratio cases are shown, the order of increasing efficiency is $J = 0.792$, $J = 0.743$, $J = 0.572$, $J = 0.691$ and $J = 0.635$. This indicates that either too low or too high dynamic pressure ratio debases combustion efficiency in a specific configuration. $J = 0.572$ case shows slightly deviated result by performing better at upstream while slowing down the efficiency growth at downstream. In figure 34 where constant dynamic pressure ratio and varying fuel total temperature cases are shown, the trend is quite clear that increasing fuel temperature results in higher combustion efficiency near cavity leading edge. These trends could be determined more easily by plotting combustion efficiency with respect to independent variables. figure 35 and 36 show combustion efficiency at certain x-positions. $x = 0.0955\,\text{m}$ data shows distinct trend. It is readily deducted from the fact that higher temperature leads to higher reaction rate in general. After that, dispersed values gathers again far downstream. This behavior can be explained with mixing efficiency results.

Constant fuel total temperature and varying dynamic pressure ratio cases are shown in figure 38. Their order of better mixing efficiency is almost identical to that of combustion. In contrast, as shown in figure 39, mixing efficiency of constant dynamic pressure ratio and varying fuel total temperature cases is different from combustion counterpart. Lower fuel temperature results in higher mixing efficiency in general. Figure 40 represents quite similar plotting with figure 35. This indicates strong relationship between two efficiencies in case of varying dynamic presssure ratio. In contrast, Figure 41 has slightly different tendency. High temperature results in reduced mixing efficiency at both upstream and downstream. This is in agreement with argument of Wendt et al.[11] because velocity of fuel jet differs greater with that of air flow as fuel temperature becomes low. Finally, pure active methane cases are shown in figure 37. $T_t = 400\,\text{K}$ case and $T_t = 600\,\text{K}$ case show the best efficiency at upstream and downstream, respectively. The results above reveal that $T_t = 400\,\text{K}$ case show good mixing performance due to low fuel temperature and $T_t = 600\,\text{K}$ case due to optimum dynamic pressure ratio.
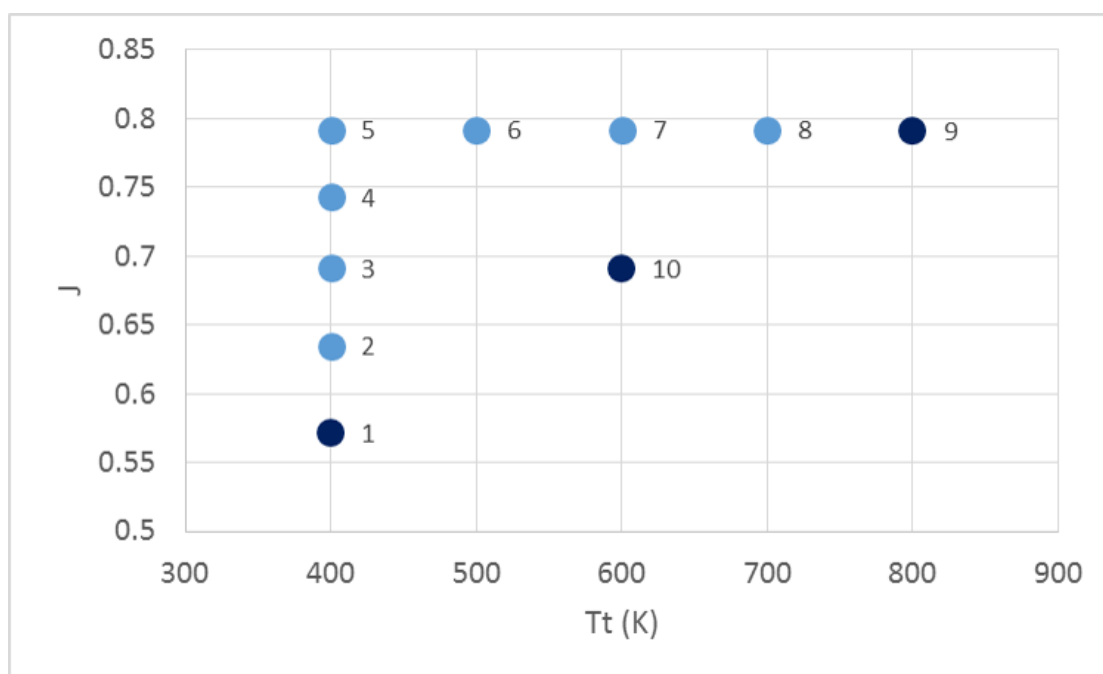
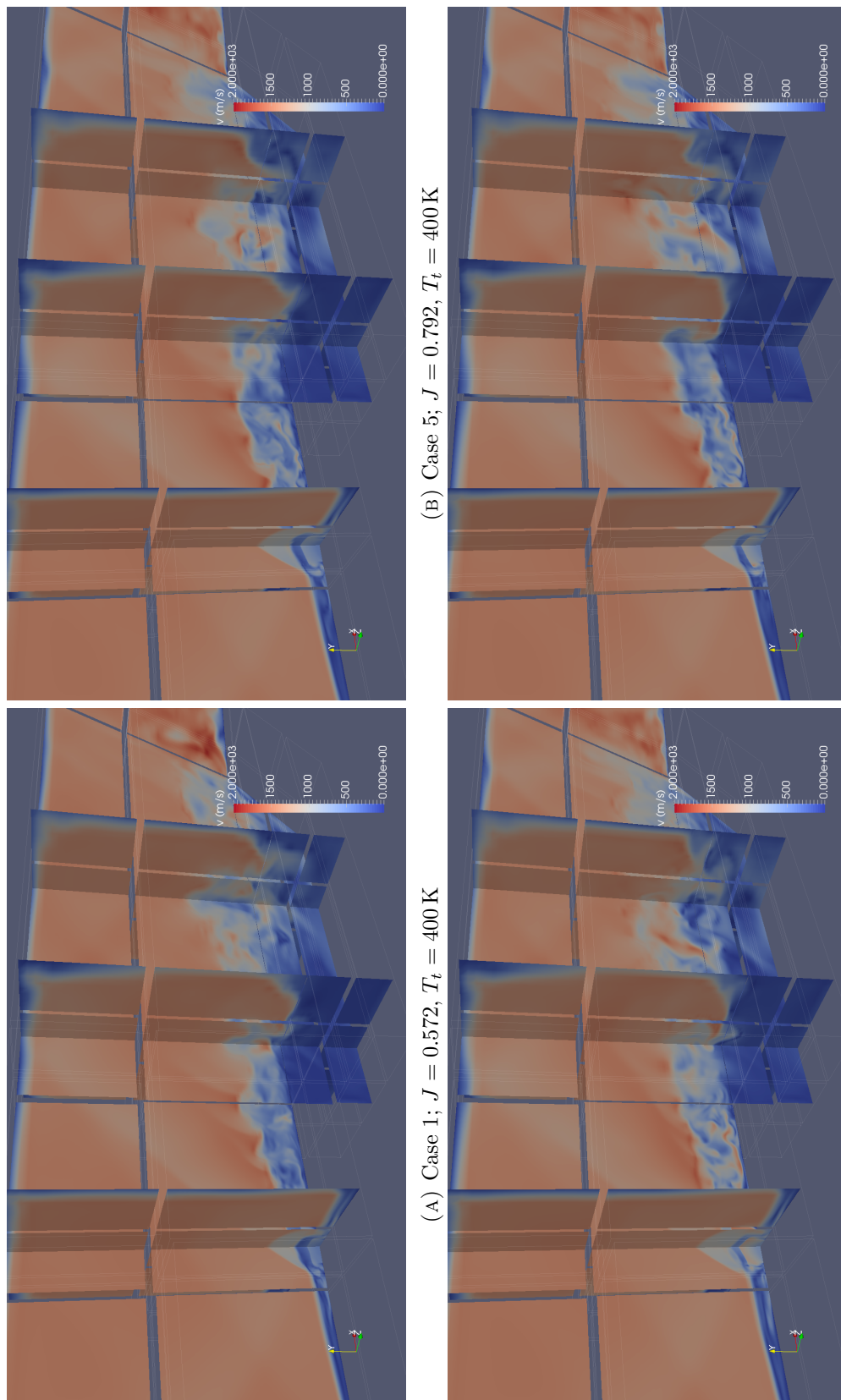FIGURE 18: Comparison of each cases by their dynamic pressure ratio and total temperature

(A) Case 1; $J = 0.572$, $T_t = 400\,\mathrm{K}$

(B) Case 5; $J = 0.792$, $T_t = 400\,\mathrm{K}$

(C) Case 9; $J = 0.792$, $T_t = 800\,\mathrm{K}$

(D) Case 10; $J = 0.691$, $T_t = 600\,\mathrm{K}$

FIGURE 19: Velocity distribution at $t = 185\,\mathrm{\mu s}$

(A) Case 1; $J = 0.572$, $T_t = 400\,\mathrm{K}$

(B) Case 5; $J = 0.792$, $T_t = 400\,\mathrm{K}$

(C) Case 9; $J = 0.792$, $T_t = 800\,\mathrm{K}$

(D) Case 10; $J = 0.691$, $T_t = 600\,\mathrm{K}$
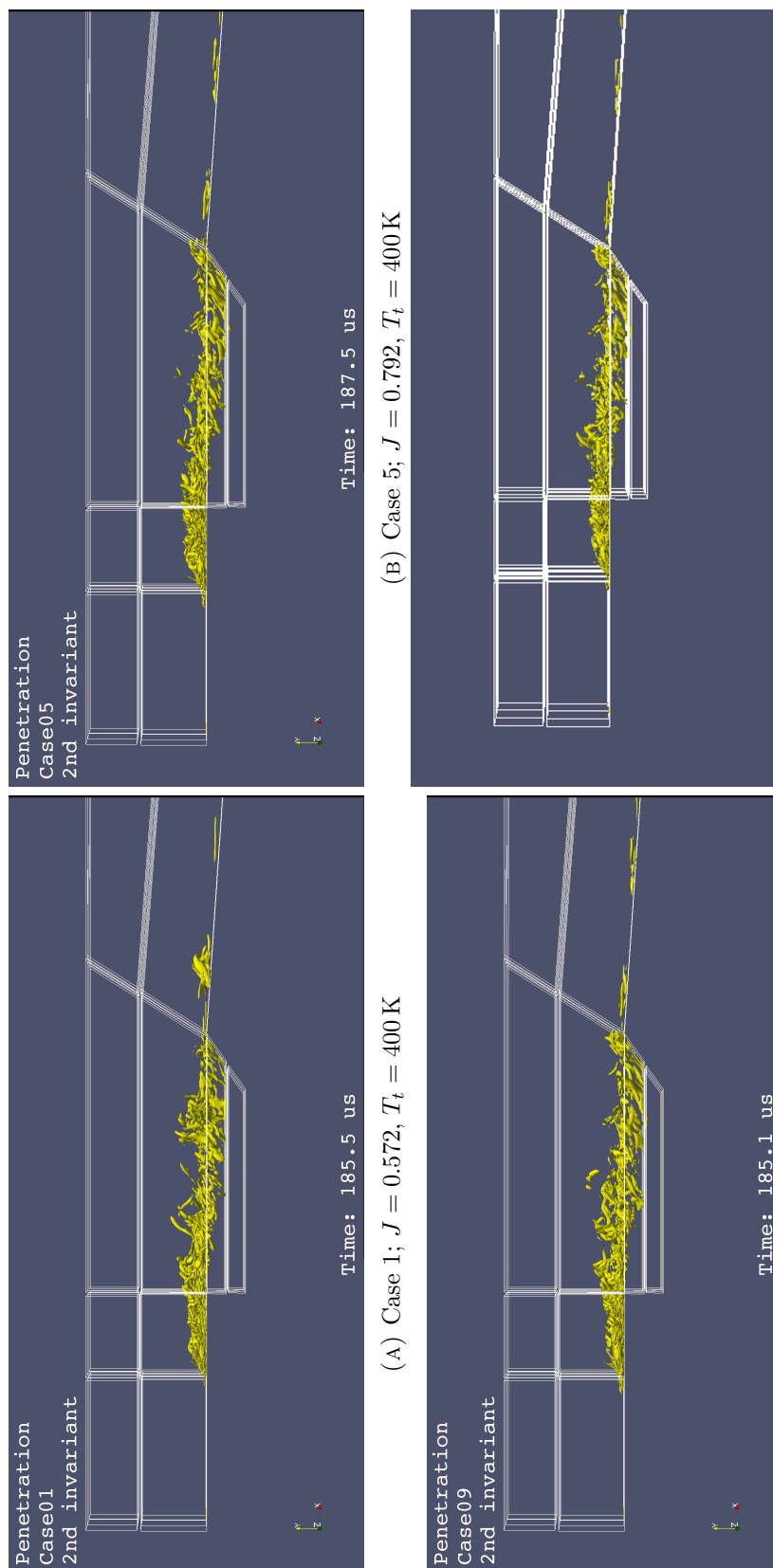
FIGURE 20: Contour of second invariant of velocity gradient tensor at $t = 185\,\mu\mathrm{s}$
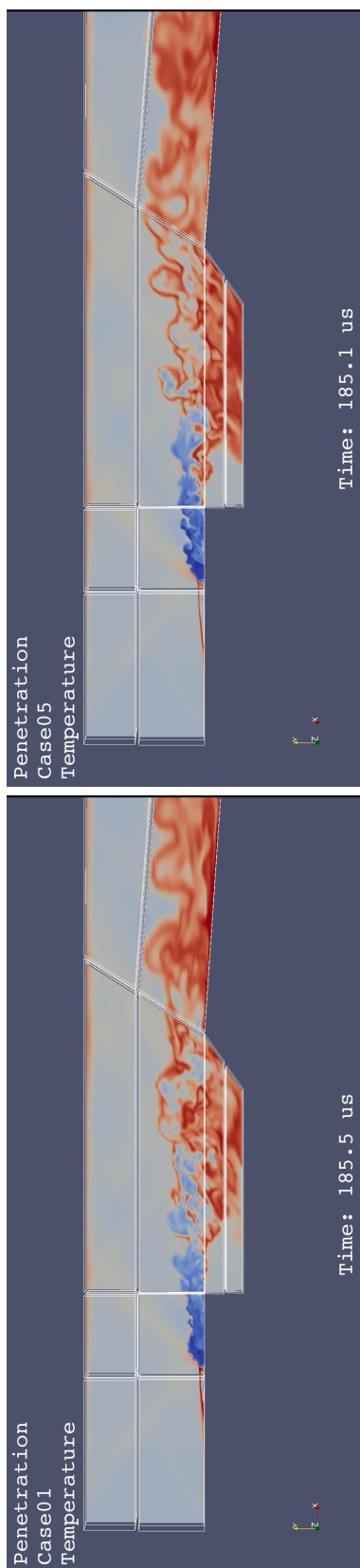
(A) Case 1; $J = 0.572$, $T_t = 400\,\mathrm{K}$
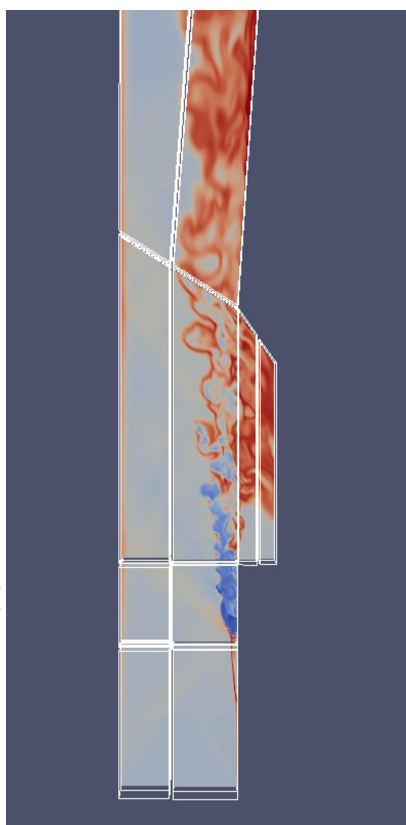
(B) Case 5; $J = 0.792$, $T_t = 400\,\mathrm{K}$
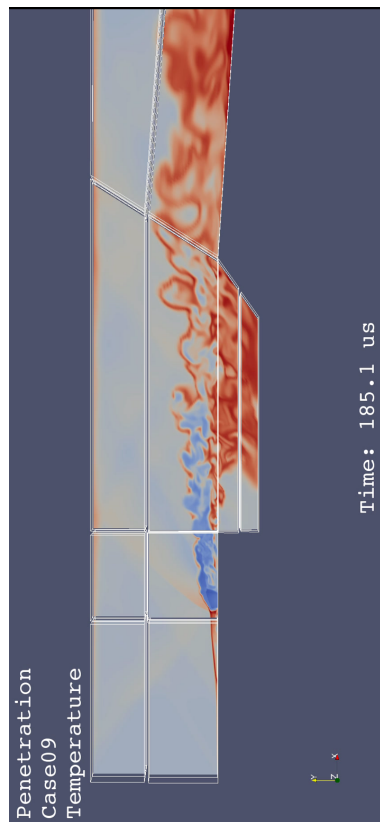
(C) Case 9; $J = 0.792$, $T_t = 800\,\mathrm{K}$

(D) Case 10; $J = 0.691$, $T_t = 600\,\mathrm{K}$

FIGURE 21: Temperature instantaneous distribution on mid-plane at $z = 15\,\mathrm{mm}$ and $t = 185\,\mathrm{\mu s}$

(A) Case 1; $J = 0.572$, $T_t = 400\,\mathrm{K}$

(B) Case 5; $J = 0.792$, $T_t = 400\,\mathrm{K}$

(C) Case 9; $J = 0.792$, $T_t = 800\,\mathrm{K}$

(D) Case 10; $J = 0.691$, $T_t = 600\,\mathrm{K}$
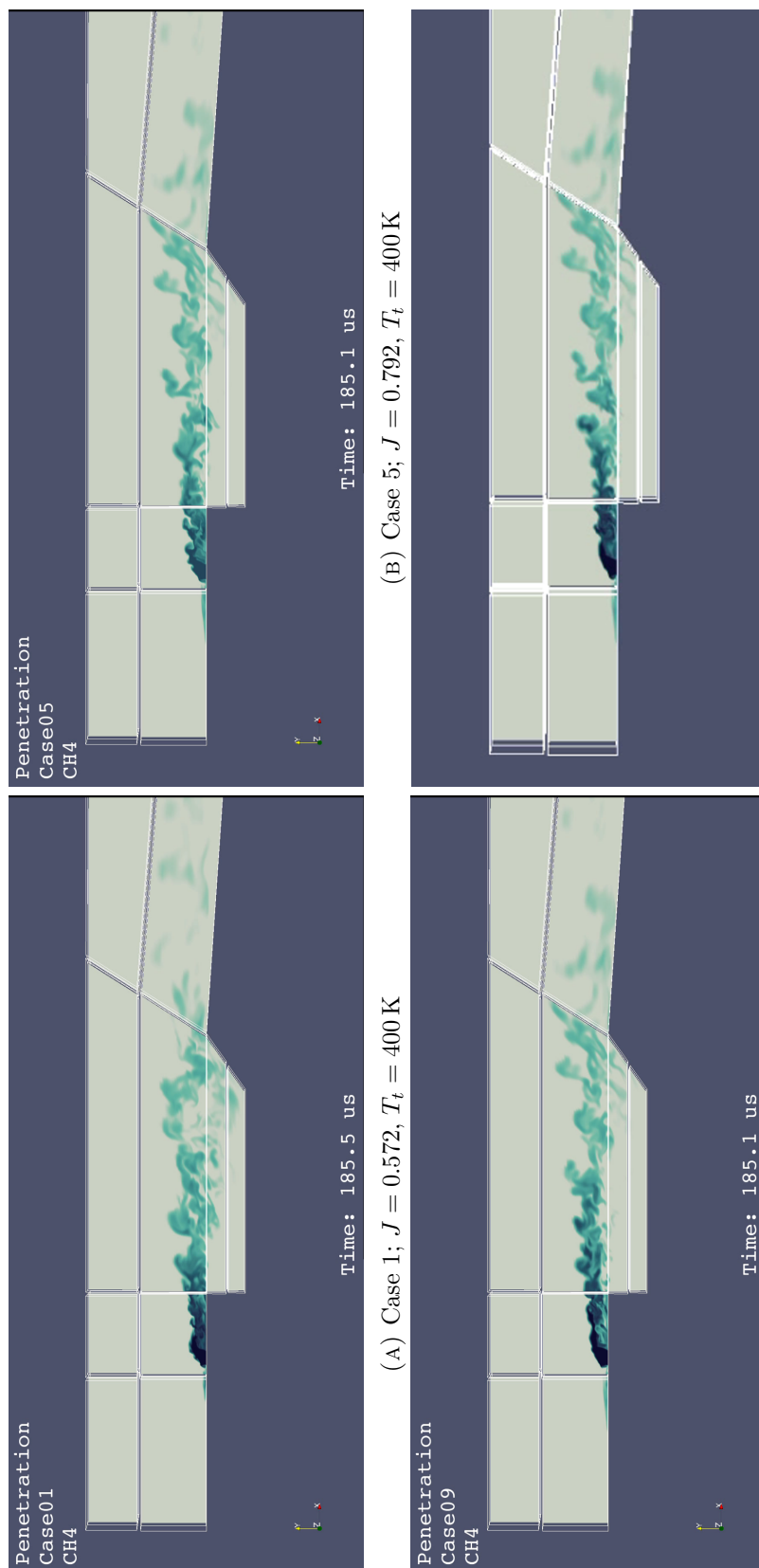
FIGURE 22: Active methane instantaneous distribution on mid-plane at $z = 15\,\mathrm{mm}$ and $t = 185\,\mathrm{\mu s}$

(A) Case 1; $J = 0.572$, $T_t = 400\,\mathrm{K}$

(B) Case 5; $J = 0.792$, $T_t = 400\,\mathrm{K}$

(C) Case 9; $J = 0.792$, $T_t = 800\,\mathrm{K}$

(D) Case 10; $J = 0.691$, $T_t = 600\,\mathrm{K}$
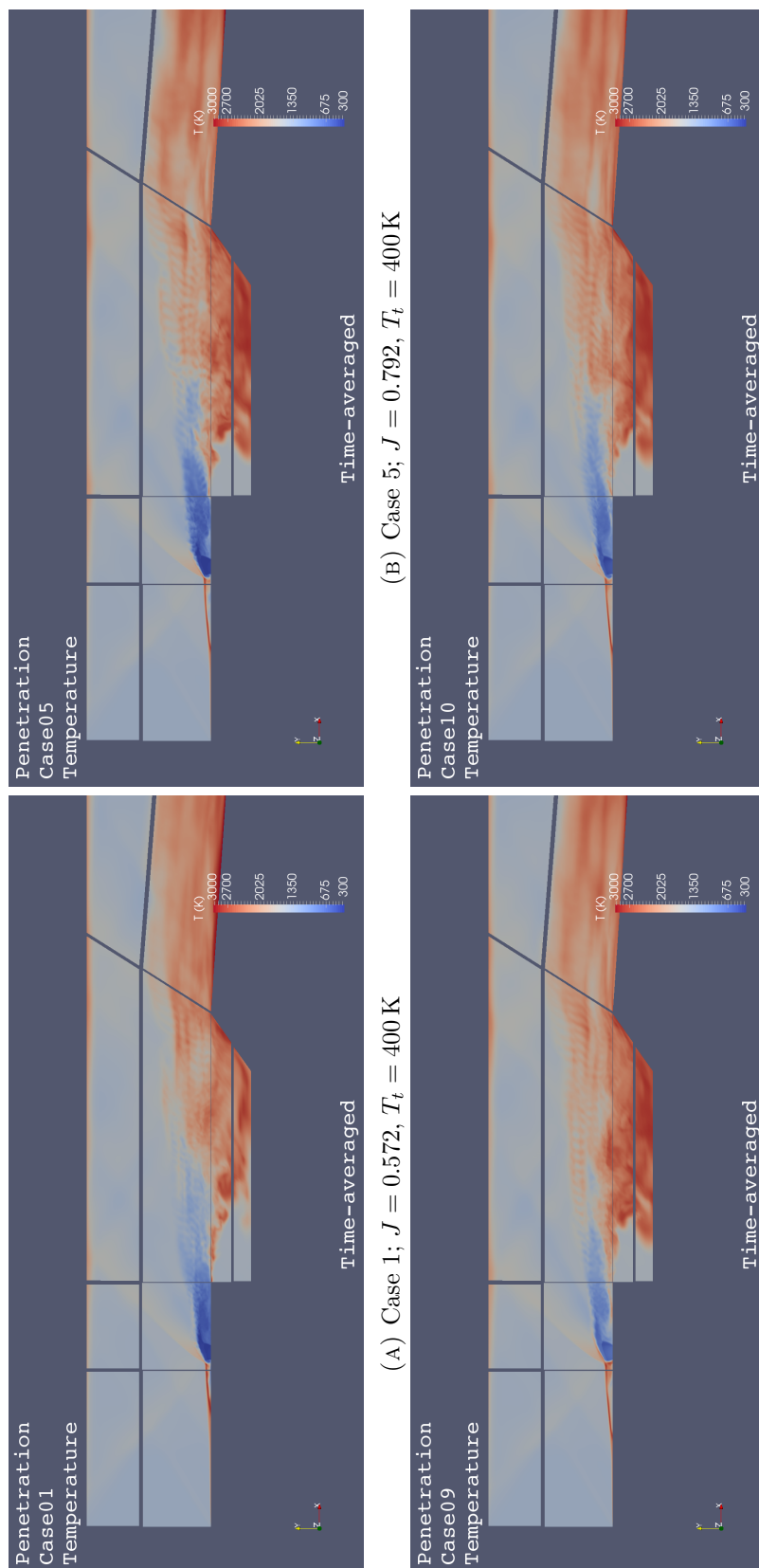
FIGURE 23: Temperature time-averaged distribution on mid-plane at $z = 15\,\mathrm{mm}$

(A) Case 1; $J = 0.572$, $T_t = 400\,\mathrm{K}$

(B) Case 5; $J = 0.792$, $T_t = 400\,\mathrm{K}$

(C) Case 9; $J = 0.792$, $T_t = 800\,\mathrm{K}$

(D) Case 10; $J = 0.691$, $T_t = 600\,\mathrm{K}$
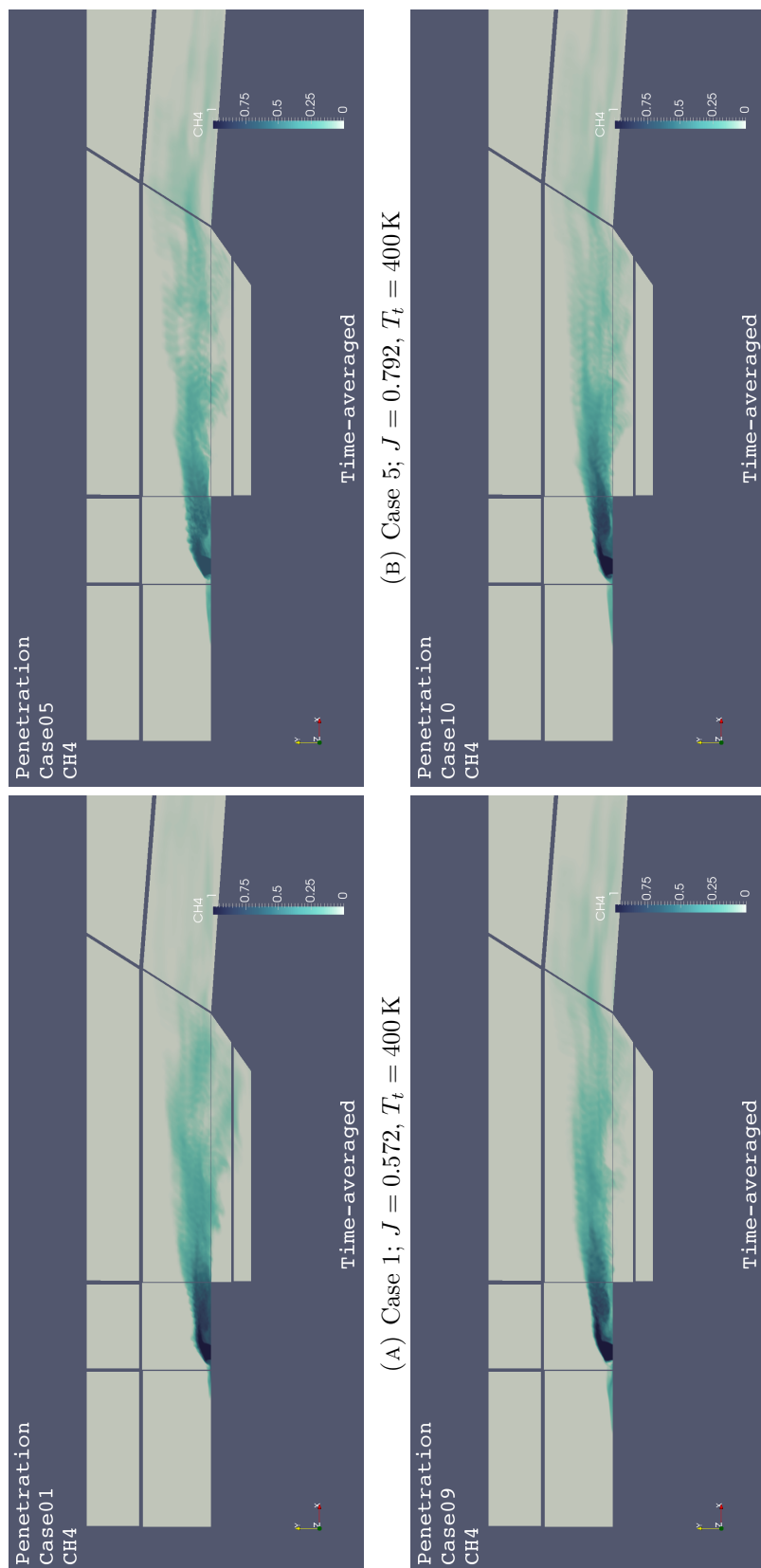
FIGURE 24: Active methane time-averaged distribution on mid-plane at $z = 15\,\mathrm{mm}$
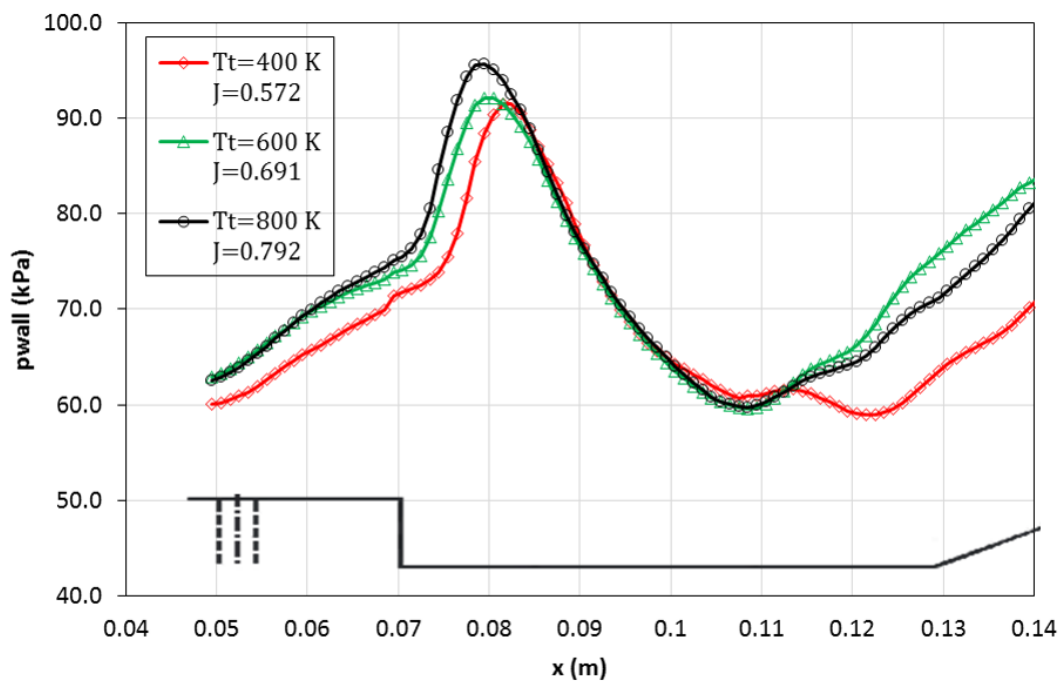
FIGURE 25: Pressure distribution on the middle line of the combustor upper wall of pure active methane cases
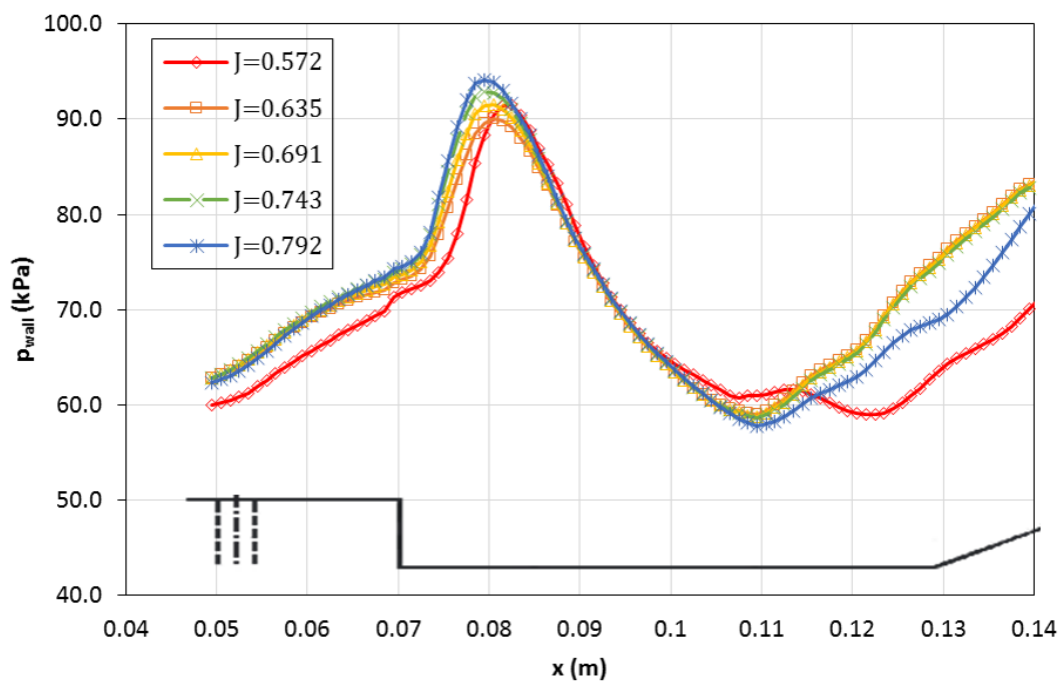
FIGURE 26: Pressure distribution on the middle line of the combustor upper wall of $T_t = 400\,\mathrm{K}$ cases
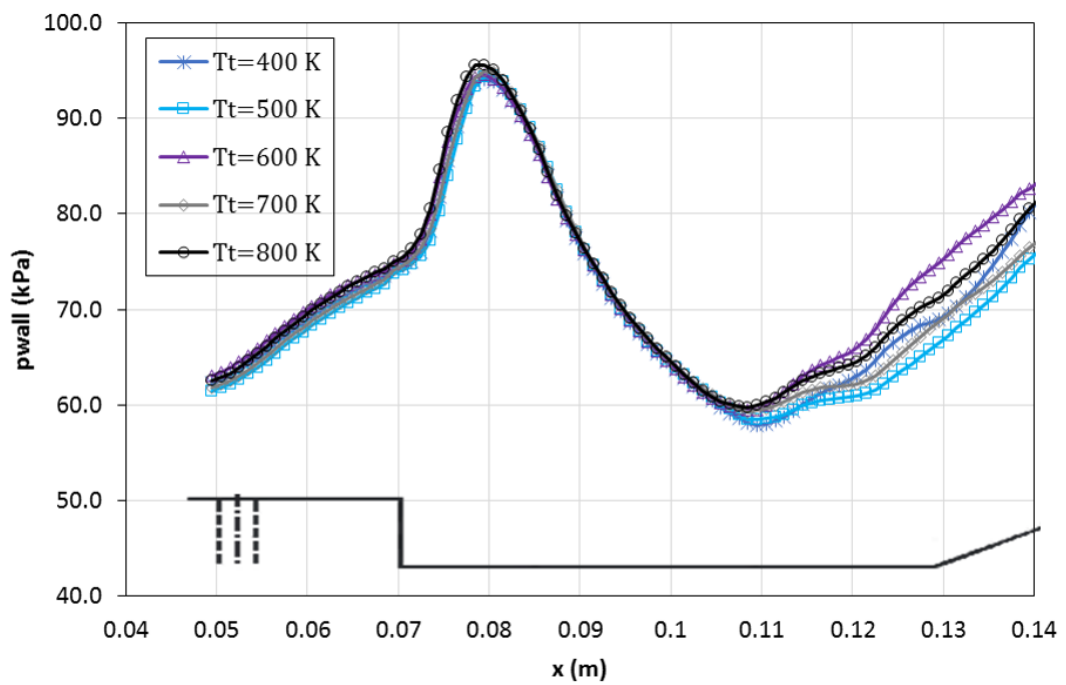
FIGURE 27: Pressure distribution on the middle line of the combustor upper wall of $J = 0.792$ cases

(A) Case 1; $J = 0.572$, $T_t = 400\,\mathrm{K}$

(B) Case 2; $J = 0.792$, $T_t = 400\,\mathrm{K}$

(C) Case 9; $J = 0.792$, $T_t = 800\,\mathrm{K}$
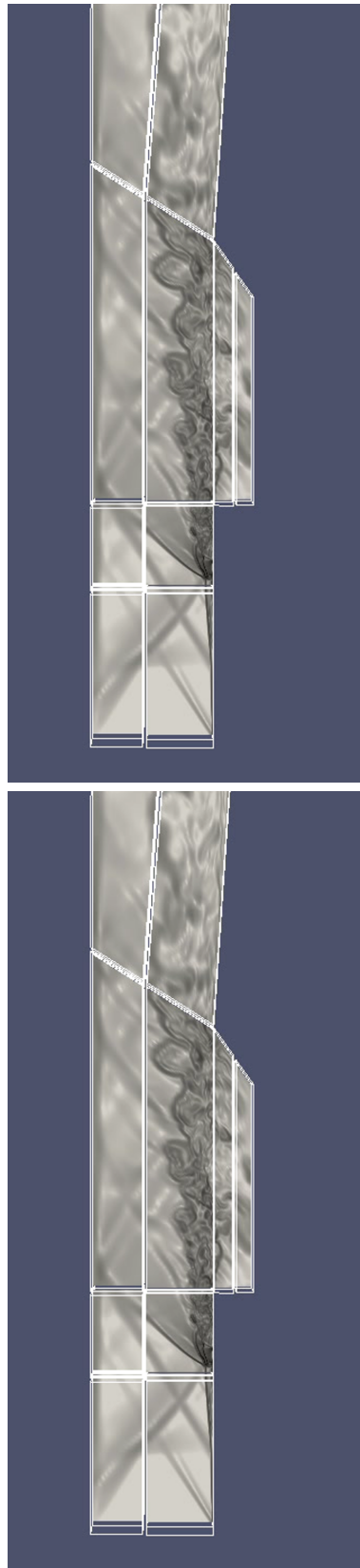
(D) Case 10; $J = 0.691$, $T_t = 600\,\mathrm{K}$
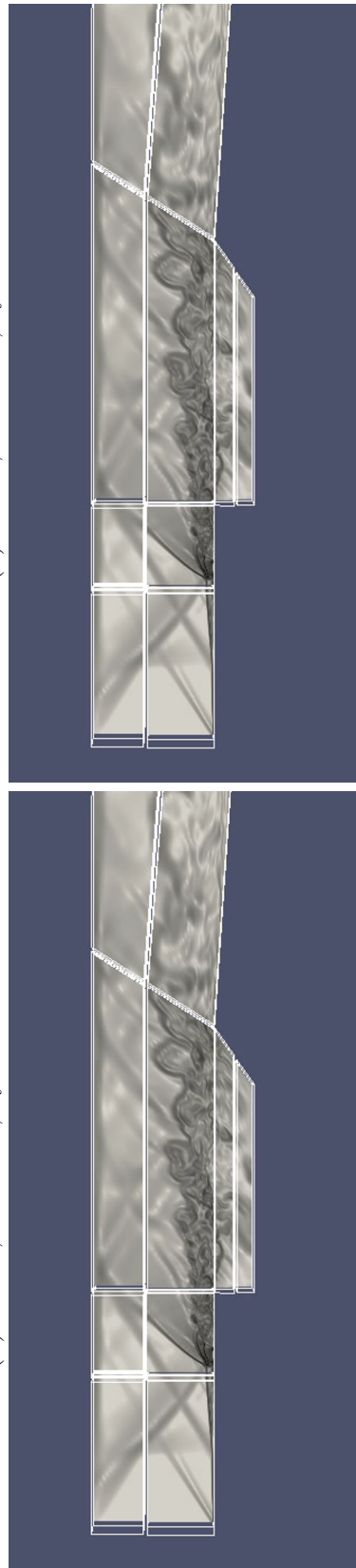
FIGURE 28: Instantaneous numerical Schlieren images at $t = 185\,\mathrm{\mu s}$
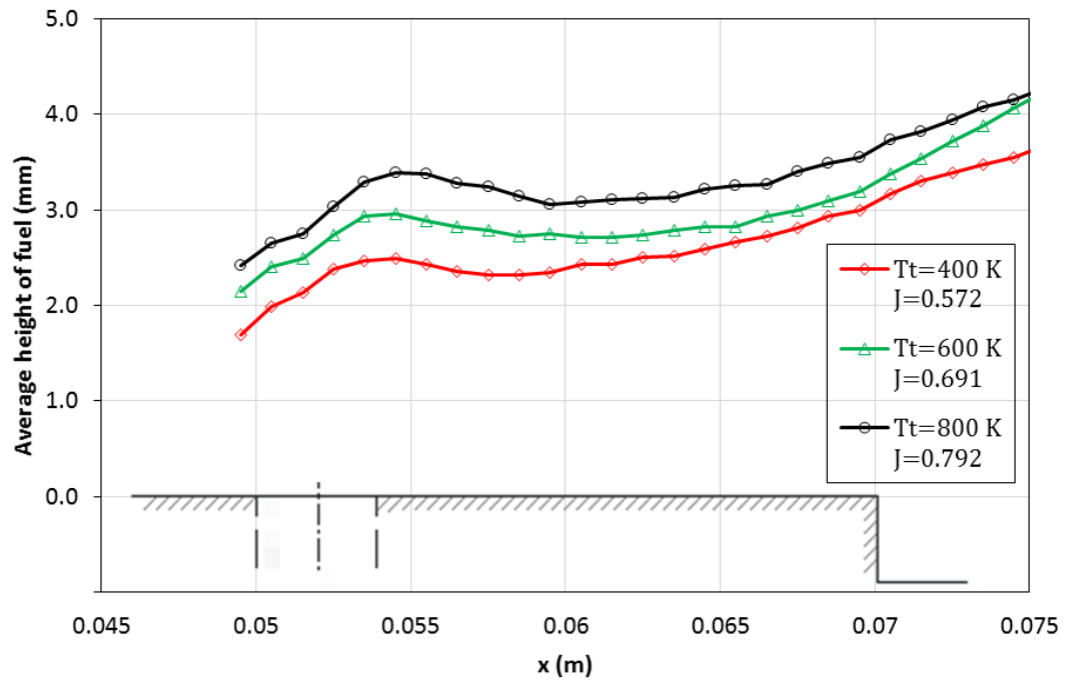
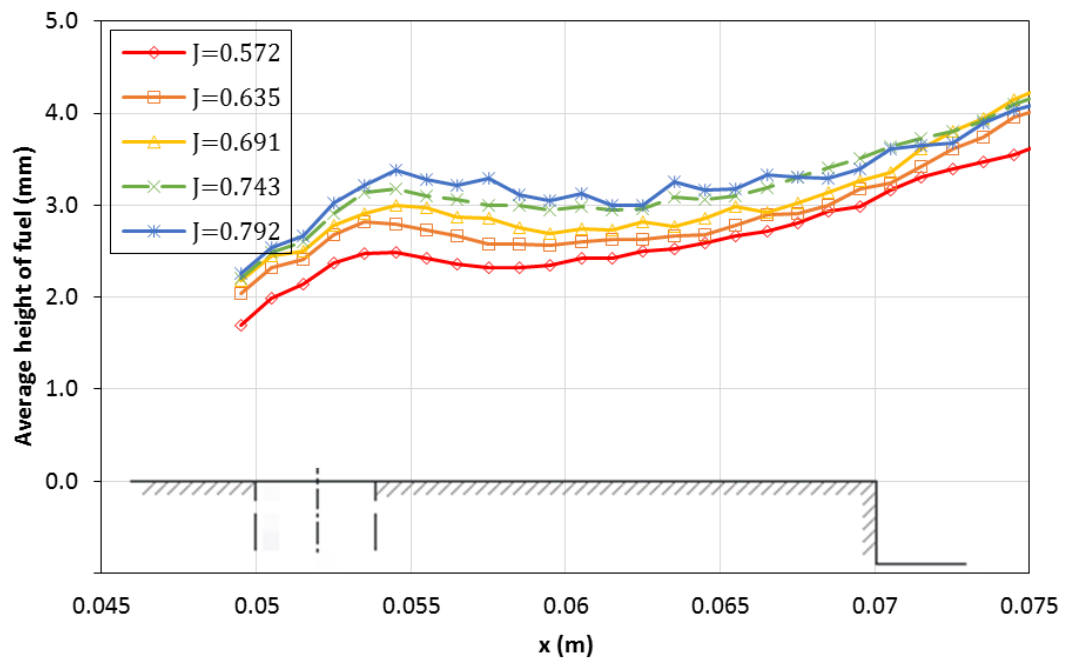FIGURE 29: Penetration after fuel injection hole of pure active methane cases

FIGURE 30: Penetration after fuel injection hole of $T_t = 400\,\mathrm{K}$ cases
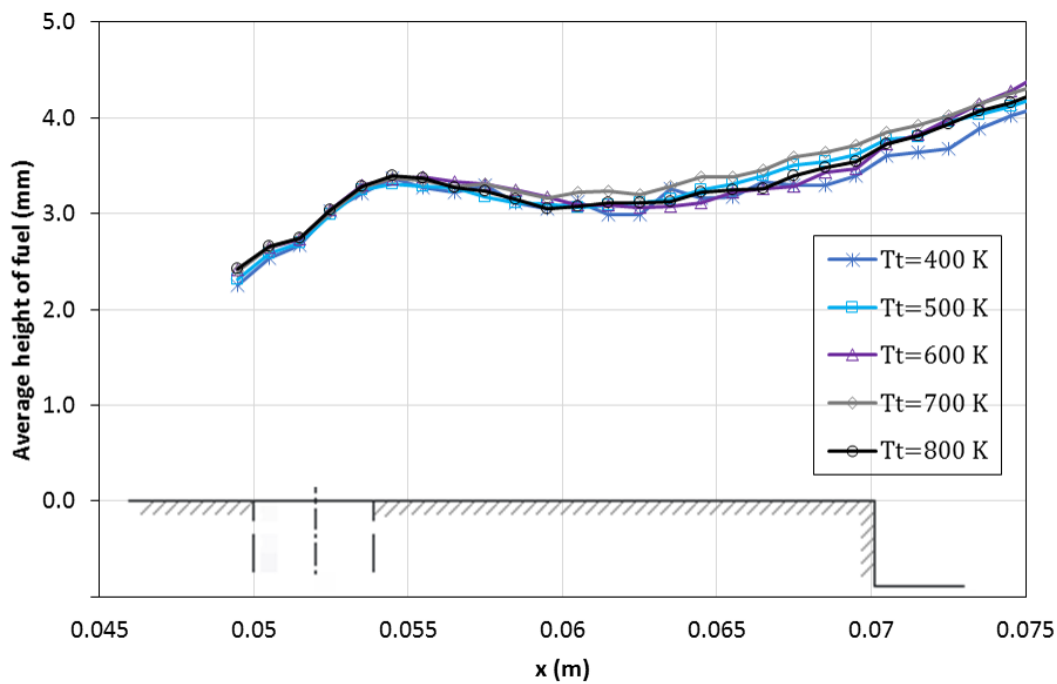
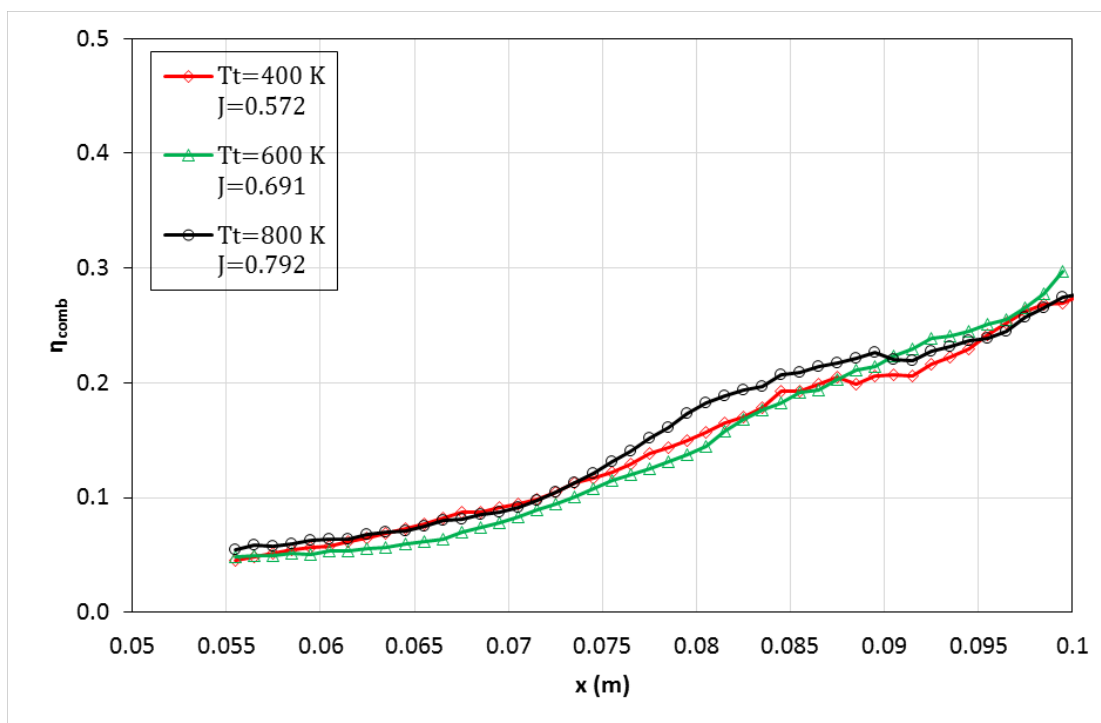FIGURE 31: Penetration after fuel injection hole of $J = 0.792$ cases
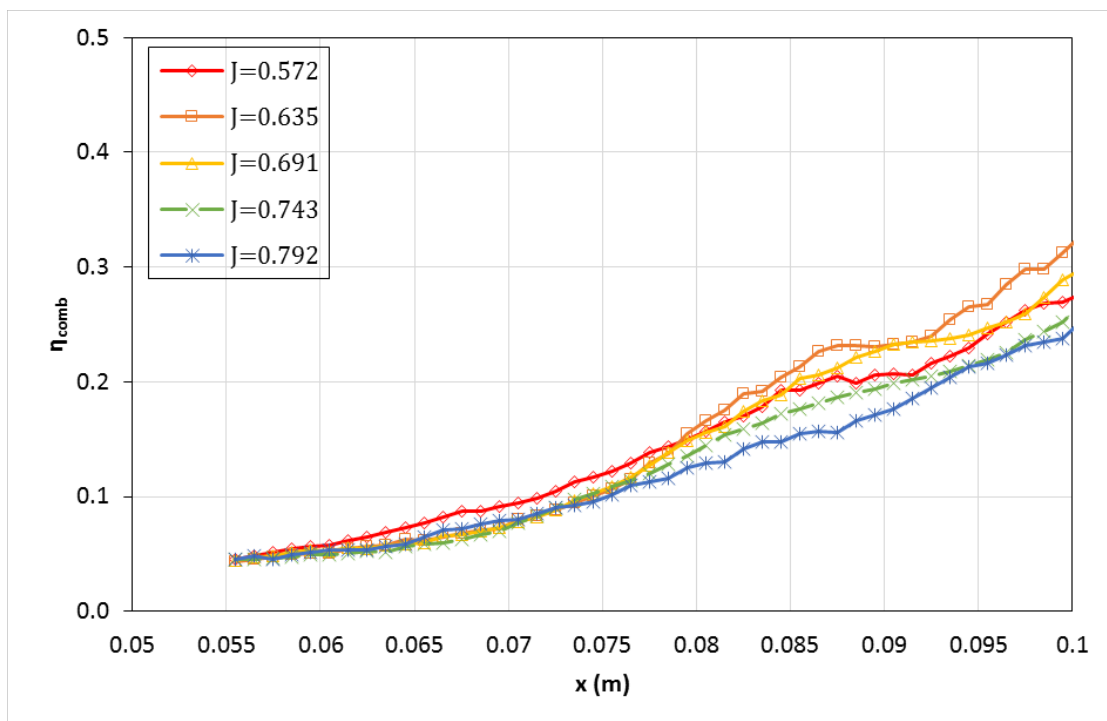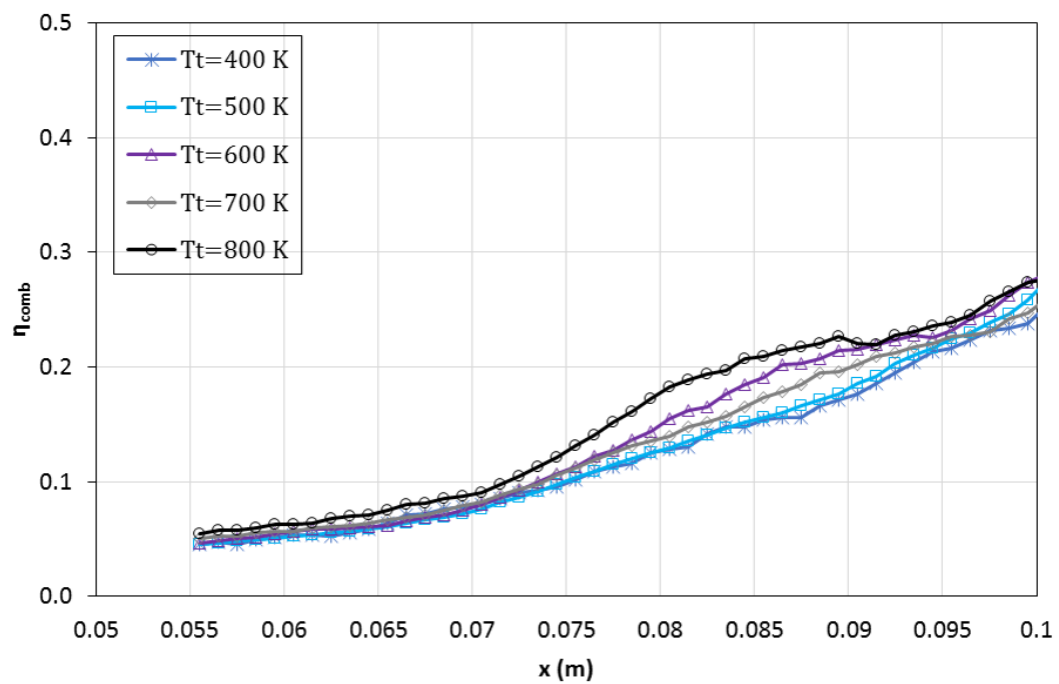

FIGURE 32: Combustion efficiency of pure active methane cases

FIGURE 33: Combustion efficiency of $T_t = 400\,\mathrm{K}$ cases

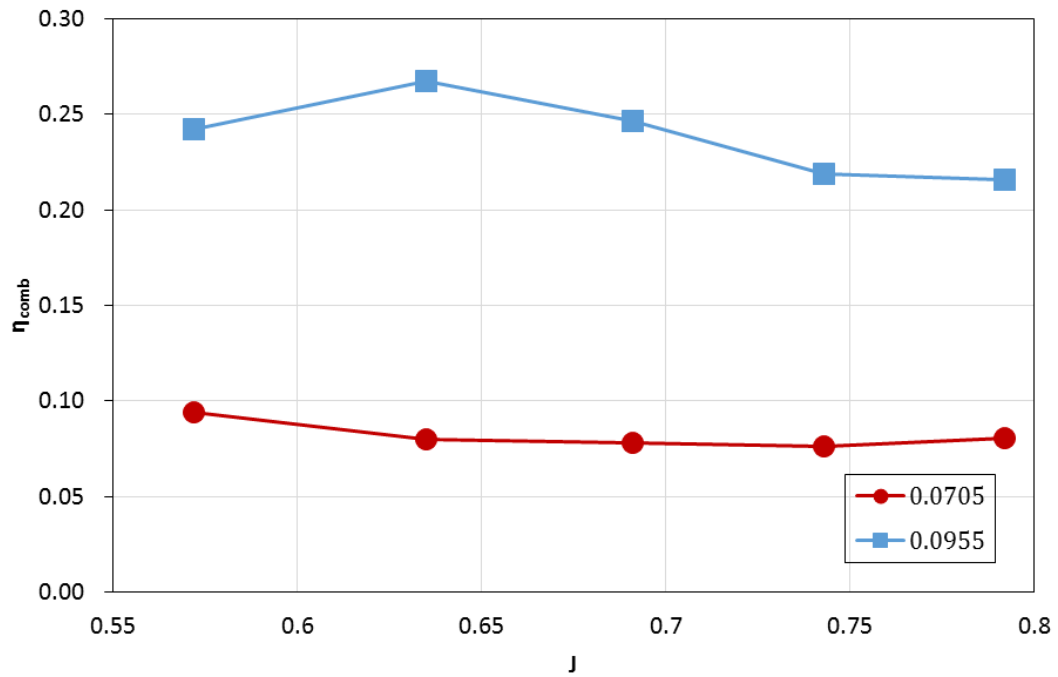FIGURE 34: Combustion efficiency of $J = 0.792$ cases

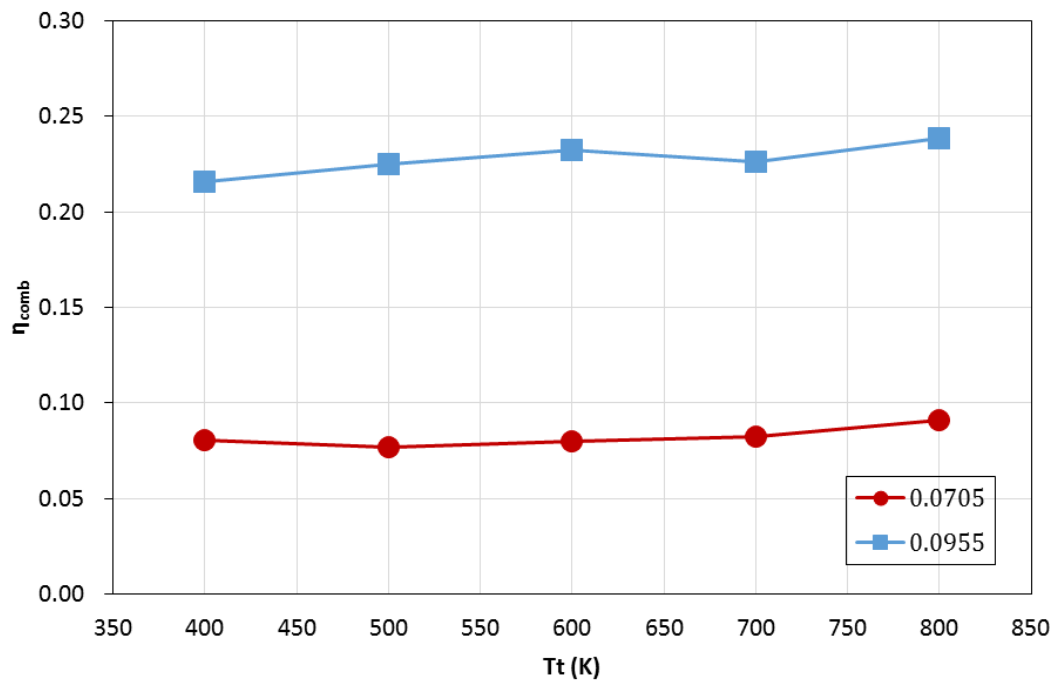FIGURE 35: Combustion efficiency of $T_t = 400\,\mathrm{K}$ cases at two positions

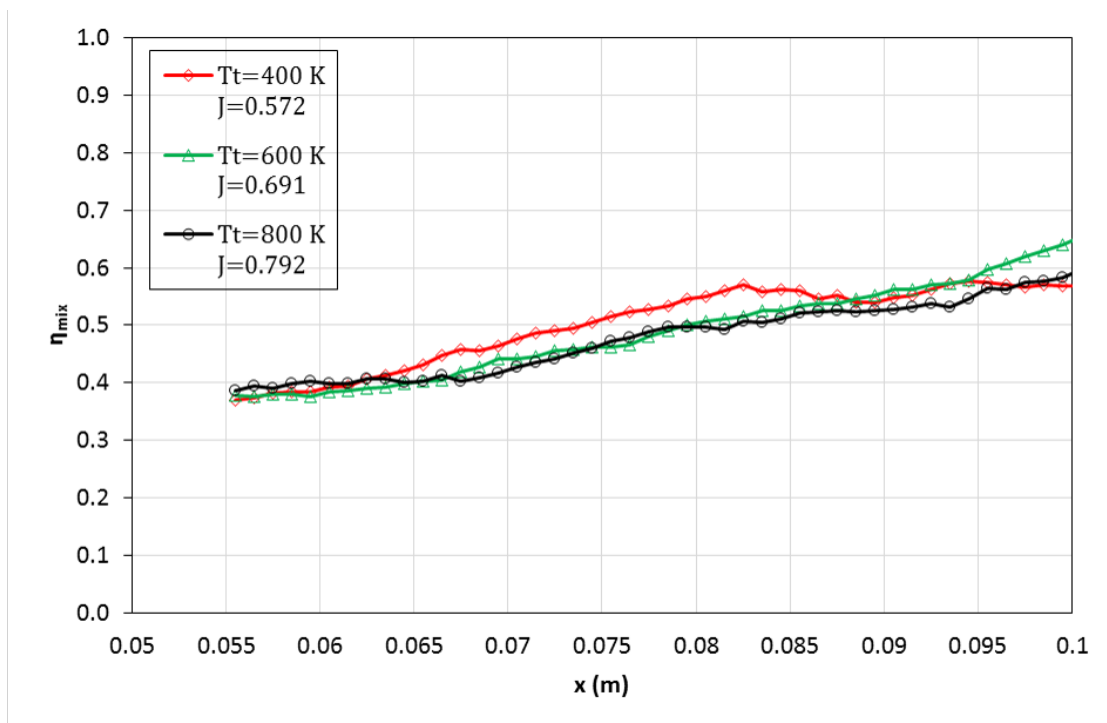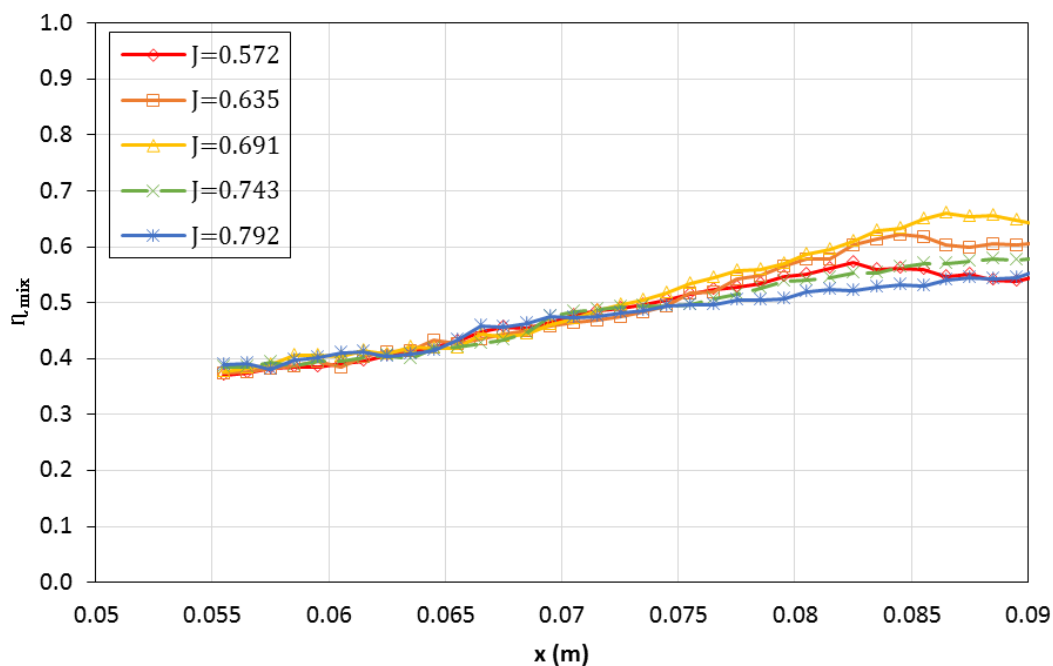FIGURE 36: Combustion efficiency of $J = 0.792$ cases at two positions

FIGURE 37: Mixing efficiency of pure active methane cases

FIGURE 38: Mixing efficiency of $T_t = 400\,\text{K}$ cases
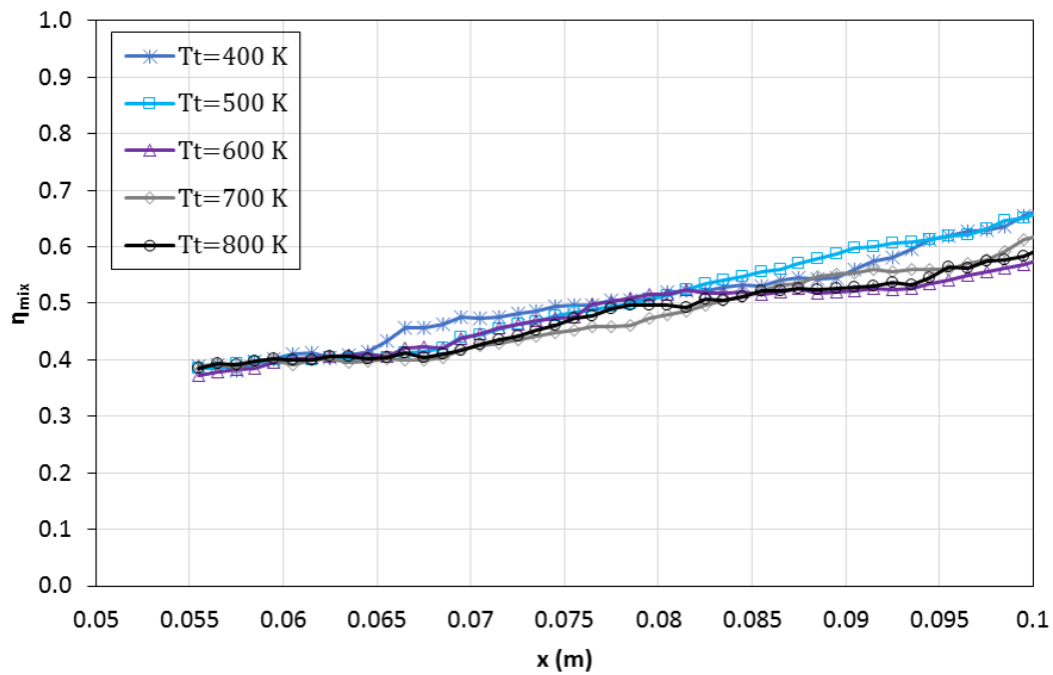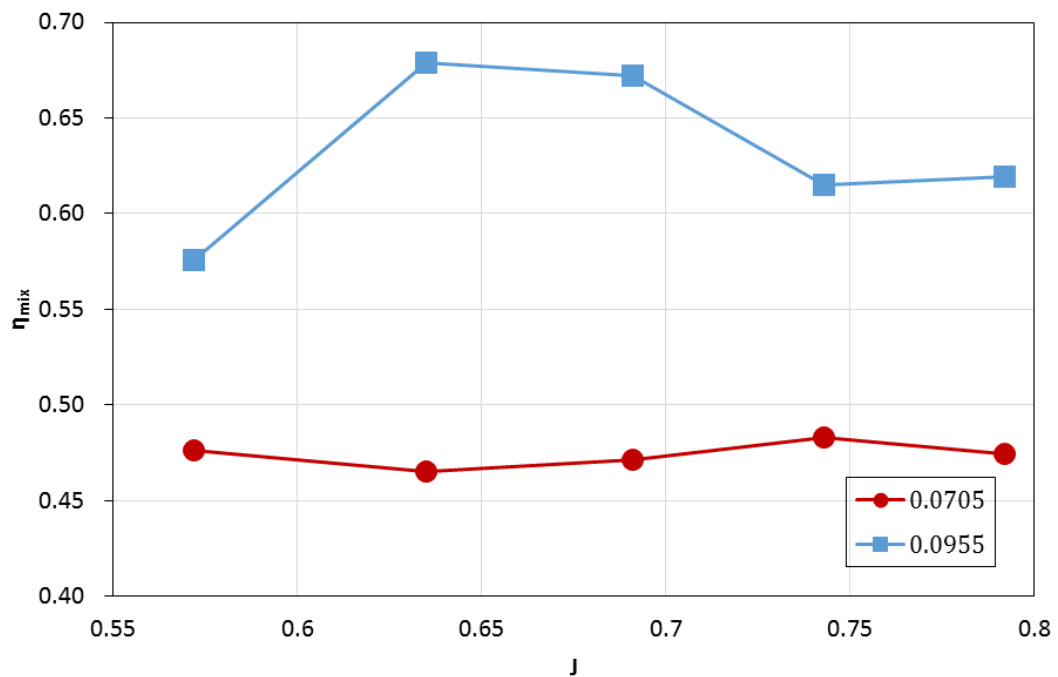
FIGURE 39: Mixing efficiency of $J = 0.792$ cases

FIGURE 40: Mixing efficiency of $T_t = 400\,\mathrm{K}$ cases at two positions
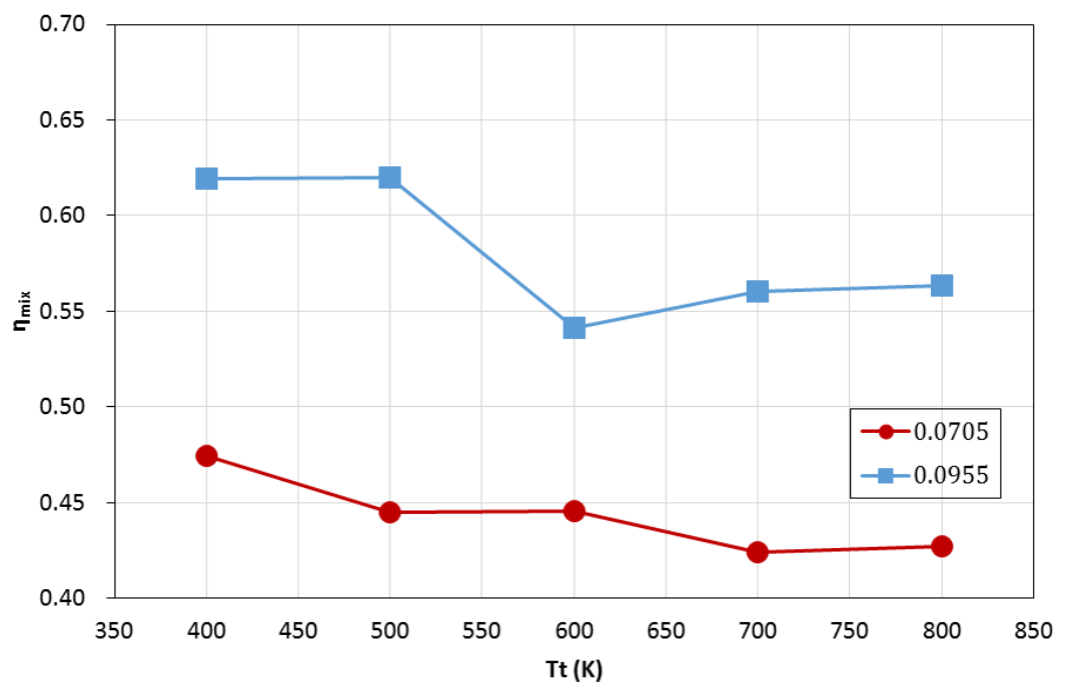
FIGURE 41: Mixing efficiency of $J = 0.792$ cases at two positions

4.4 Conclusion

The behavior of supersonic methane fuel jet combustion with respect to fuel total temperature has been numerically investigated by revealing effects of dynamic pressure ratio change between fuel jet and air flow and fuel temperature change. For mixing and combustion, dynamic pressure ratio and fuel temperature affected those efficiencies in different way. Fuel temperature did not altered penetration characteristics significantly. Higher fuel temperature expedited chemical reaction rate, while lower temperature enhanced mixing in downstream. This resulted in converged combustion efficiency. Dynamic pressure ratio affects penetration mainly. Extreme dynamic pressure ratio did not resulted in better mixing efficiency, and this was carried over to combustion efficiency.

For better controllability of scramjet engine combustor, penetration, mixing and reactivity of the fuel are acting in different way but influences each other. In this research, those factors were investigated in separated manner, and this information could be extended to fundamental knowledge for flame control of supersonic combustor.

Chapter 5

Summary

Development of reliable scramjet engine combustor rises as an important task for hypersonic flight mission. Hydrocarbon fuel could be safe, economic and versatile candidate for scramjet. Therefore physical and chemical phenomena related to supersonic hydrocarbon fuel injection attracts attention from all over the world.

In order to investigate those phenomena, numerical analyses have been conducted. In-house developed simulation code which is based on governing equations of fluid mechanics and combustion theory. Since Navier-Stokes equation contains hyperbolic partial differential equation, appropriate numerical methodologies has been applied to the computational code.

Several methane reaction modelings have been conducted and their results were compared. Frozen, infinitely fast, Jones-Lindstedt and Li-Williams reaction modeling were selected as candidates. While frozen and infinitely fast chemistry have been two extrema among applicable modeling, Jones-Lindstedt and Li-Williams have shown advantages in different aspect.

The behavior of supersonic methane fuel jet combustion with respect to fuel total temperature has been investigated by revealing effects of dynamic pressure ratio and fuel temperature change. Those factors were treated in separated manner, and through this research, effects of penetration, mixing and reactivity could be studied for better scramjet combustor control.

Bibliography

[1] M. R. Gruber, A. S. Nejadt, T. H. Chen, and J. C. Dutton. Mixing and penetration studies of sonic jets in a mach 2 freestream. *Journal of Propulsion and Power*, 11 (2):315–323, 1995. ISSN 0748-4658. doi: 10.2514/3.51427. URL `http://dx.doi.org/10.2514/3.51427http://arc.aiaa.org/doi/abs/10.2514/3.51427`.

[2] A. Ben-Yakar, M. G. Mungal, and R. K. Hanson. Time evolution and mixing characteristics of hydrogen and ethylene transverse jets in supersonic crossflows. *Physics of Fluids*, 18(2):026101, 2006. ISSN 10706631. doi: 10.1063/1.2139684.

[3] Sang Hun Kang, Yang Ji Lee, Soo Seok Yang, Michael K. Smart, and Milinda K. Suraweera. Cowl and cavity effects on mixing and combustion in scramjet engines. *Journal of Propulsion and Power*, 27(6):1169–1177, 2011. ISSN 0748-4658 1533-3876. doi: 10.2514/1.48818.

[4] Peter Gerlinger, Peter Stoll, Markus Kindler, Fernando Schneider, and Manfred Aigner. Numerical investigation of mixing and combustion enhancement in supersonic combustors by strut induced streamwise vorticity. *Aerospace Science and Technology*, 12(2):159–168, 2008. ISSN 12709638. doi: 10.1016/j.ast.2007.04.003.

[5] J. H. Kim, Y. Yoon, I. S. Jeung, H. Huh, and J. Y. Choi. Numerical study of mixing enhancement by shock waves in model scramjet engine. *Aiaa Journal*, 41

(6):1074–1080, 2003. ISSN 0001-1452. doi: Doi10.2514/2.2047. URL `<GotoISI>:`
`//WOS:000183246900010`. 685EB Times Cited:11 Cited References Count:20.

[6] M. R. Gruber, J. M. Donbar, C. D. Carter, and K. Y. Hsu. Mixing and combustion
studies using cavity-based flameholders in a supersonic flow. *Journal of Propulsion
and Power*, 20(5):769–778, 2004. ISSN 0748-4658 1533-3876. doi: 10.2514/1.5360.

[7] Jianhan Liang, Cheng Gong, Sun Ming-bo, and Zhou Jin. Hybrid rans/les simula-
tion of the fuel injection and mixing process in a supersonic combustor with cavity
flame-holder. 2013. doi: 10.2514/6.2013-3698.

[8] M. Berglund and C. Fureby. Les of supersonic combustion in a scramjet engine
model. *Proceedings of the Combustion Institute*, 31(2):2497–2504, 2007. ISSN
15407489. doi: 10.1016/j.proci.2006.07.074.

[9] C. Fureby, M. Chapuis, E. Fedina, and S. Karl. Cfd analysis of the hyshot ii scramjet
combustor. *Proceedings of the Combustion Institute*, 33(2):2399–2405, 2011. ISSN
15407489. doi: 10.1016/j.proci.2010.07.055.

[10] Junya Watanabe, Toshinori Kouchi, Kenichi Takita, and Goro Masuya. Charac-
teristics of hydrogen jets in supersonic crossflow: Large-eddy simulation study.
Journal of Propulsion and Power, 29(3):661–674, 2013. ISSN 0748-4658 1533-3876.
doi: 10.2514/1.b34521.

[11] M. N. Wendt, R. J. Stalker, and P. A. Jacobs. Fuel stagnation temperature effects
on mixing with supersonic combustion flows. *Journal of Propulsion and Power*, 13
(2):274–280, 1997. ISSN 0748-4658 1533-3876. doi: 10.2514/2.5159.

[12] T. Poinsot and D. Veynante. *Theoretical and numerical combustion*. Edwards, 2005.
ISBN 1-930217-10-2.

[13] Massimo Germano, Ugo Piomelli, Parviz Moin, and William H. Cabot. A dynamic subgrid-scale eddy viscosity model. *Physics of Fluids A: Fluid Dynamics*, 3(7):1760, 1991. ISSN 08998213. doi: 10.1063/1.857955.

[14] M. S. Liou and C. J. Steffen. A new flux splitting scheme. *Journal of Computational Physics*, 107(1):23–39, 1993. ISSN 0021-9991. doi: DOI10.1006/jcph.1993.1122. URL `<GotoISI>://WOS:A1993LK45500003`. Lk455 Times Cited:348 Cited References Count:19.

[15] P. L. Roe. Approximate riemann solvers, parameter vectors, and difference schemes. *Journal of Computational Physics*, 43(2):357–372, 1981. ISSN 0021-9991. doi: http://dx.doi.org/10.1016/0021-9991(81)90128-5. URL `http://www.sciencedirect.com/science/article/pii/0021999181901285`.

[16] Bram van Leer. *Flux-vector splitting for the Euler equations*, volume 170 of *Lecture Notes in Physics*, book section 66, pages 507–512. Springer Berlin Heidelberg, 1982. ISBN 978-3-540-11948-7. doi: 10.1007/3-540-11948-5_66. URL `http://dx.doi.org/10.1007/3-540-11948-5_66`.

[17] Kyu Hong Kim, Chongam Kim, and Oh-Hyun Rho. Methods for the accurate computations of hypersonic flows. *Journal of Computational Physics*, 174(1):38–80, 2001. ISSN 00219991. doi: 10.1006/jcph.2001.6873.

[18] Angelo Scandaliato and Meng-Sing Liou. Ausm-based high-order solution for euler equations. 2010. doi: 10.2514/6.2010-719.

[19] Meng-Sing Liou. A sequel to ausm, part ii: Ausm+-up for all speeds. *Journal of Computational Physics*, 214(1):137–170, 2006. ISSN 00219991. doi: 10.1016/j.jcp.2005.09.020.

[20] Meng-Sing Liou. A sequel to ausm: Ausm+. *Journal of Computational Physics*, 129(2):364–382, 1996. ISSN 0021-9991. doi: http://dx.doi.org/10.1006/jcph.1996.0256. URL `http://www.sciencedirect.com/science/article/pii/S0021999196902569http://ac.els-cdn.com/S0021999196902569/1-s2.0-S0021999196902569-main.pdf?_tid=1ef0c8ca-9a2e-11e3-906d-00000aacb35f&acdnat=1392901043_2945b6240606d9feca44f2d6be1f9d0dhttp://ac.els-cdn.com/S0021999196902569/1-s2.0-S0021999196902569-main.pdf?_tid=29e980a0-9a2e-11e3-a86c-00000aacb360&acdnat=1392901061_5144f10c1b25791d7bbab33a3c31b11bhttp://ac.els-cdn.com/S0021999196902569/1-s2.0-S0021999196902569-main.pdf?_tid=393c466e-9a2e-11e3-b2ac-00000aacb35e&acdnat=1392901087_50dc70764e8d5a1dc841ef1ef6f2e37c`.

[21] N. P. Waterson and H. Deconinck. Design principles for bounded higher-order convection schemes a unified approach. *Journal of Computational Physics*, 224 (1):182–207, 2007. ISSN 00219991. doi: 10.1016/j.jcp.2007.01.021.

[22] S. Yoon and A. Jameson. Lower-upper symmetric-gauss-seidel method for the euler and navier-stokes equations. *Aiaa Journal*, 26(9):1025–1026, 1988. ISSN 0001-1452. doi: Doi10.2514/3.10007. URL `<GotoISI>://WOS:A1988R129900001`. R1299 Times Cited:242 Cited References Count:9.

[23] P. Manna, Ramesh Behera, and Debasis Chakraborty. Liquid-fueled strut-based scramjet combustor design: A computational fluid dynamics approach. *Journal of Propulsion and Power*, 24(2):274–281, 2008. ISSN 0748-4658 1533-3876. doi: 10.2514/1.28333.

[24] Michael Emory, Vincent Terrapon, Rene Pecnik, and Gianluca Iaccarino. Characterizing the operability limits of the hyshot ii scramjet through rans simulations. 2011. doi: 10.2514/6.2011-2282.

[25] W. P. Jones and R. P. Lindstedt. Global reaction schemes for hydrocarbon combustion. *Combustion and Flame*, 73(3):233–249, 1988. ISSN 0010-2180. doi: Doi10. 1016/0010-2180(88)90021-1. URL `<GotoISI>://WOS:A1988P986600002`. P9866 Times Cited:250 Cited References Count:44.

[26] S. C. Li and F. A. Williams. Reaction mechanisms for methane ignition. *Journal of Engineering for Gas Turbines and Power*, 124(3):471, 2002. ISSN 07424795. doi: 10.1115/1.1377871.

[27] J Bonnie, BJ McBride, MJ Zehe, and S Gordon. Glenn coefficients for calculating thermodynamic properties of individual species: Report nasa. Report, TP-2002, 2002.

[28] J. Warnatz, U. Maas, and R. W. Dibble. *Combustion.* Springer, Germany, 4th edition, 2006. ISBN 3-540-25992-9 978-3-540-25992-3.

[29] G. Yu, J. G. Li, X. Y. Chang, L. H. Chen, and C. J. Sung. Fuel injection and flame stabilization in a liquid-kerosene-fueled supersonic combustor. *Journal of Propulsion and Power*, 19(5):885–893, 2003. ISSN 0748-4658. doi: Doi10.2514/ 2.6179. URL `<GotoISI>://WOS:000185629800017`. 726YU Times Cited:19 Cited References Count:20.

[30] X. J. Fan, G. Yu, J. G. Li, X. Y. Zhang, and C. J. Sung. Investigation of vaporized kerosene injection and combustion in a supersonic model combustor. *Journal of Propulsion and Power*, 22(1):103–110, 2006. ISSN 0748-4658. doi: Doi10.2514/1.

15427. URL `<GotoISI>`://WOS:000234910900012. 006QB Times Cited:11 Cited References Count:40.

[31] Bibrzycki and Poinsot. Reduced chemical kinetic mechanisms for methane combustion in o2/n2 and o2/co2 atmosphere.

[32] N. Peters. Numerical and asymptotic analysis of systematically reduced reaction schemes for hydrocarbon flames. *Lecture Notes in Physics*, 241:90–109, 1985. ISSN 0075-8450. URL `<GotoISI>`://WOS:A1985AXL8000006. Axl80 Times Cited:102 Cited References Count:13.

[33] R. W. Bilger, S. H. Starner, and R. J. Kee. On reduced mechanisms for methane-air combustion in nonpremixed flames. *Combustion and Flame*, 80(2):135–149, 1990. ISSN 0010-2180. doi: Doi10.1016/0010-2180(90)90122-8. URL `<GotoISI>`://WOS: A1990DH70100003. Dh701 Times Cited:223 Cited References Count:16.

[34] S. H. Kang, Y. J. Lee, S. S. Yang, and B. Choi. Effects of flameholder configurations on combustion in scramjet engines. *Journal of Propulsion and Power*, 28(4):739–746, 2012. ISSN 0748-4658. doi: 10.2514/1.B3432310.2514/1.59079. URL `<GotoISI>`://WOS:000306533900007. 975TH Times Cited:1 Cited References Count:14.

[35] Daniel J. Micka and James F. Driscoll. Combustion characteristics of a dual-mode scramjet combustor with cavity flameholder. *Proceedings of the Combustion Institute*, 32(2):2397–2404, 2009. ISSN 15407489. doi: 10.1016/j.proci.2008.06.192.

[36] Juan Gabriel Santiago and J. Craig Dutton. Velocity measurements of a jet injected into a supersonic crossflow. *Journal of Propulsion and Power*, 13(2):264–273, 1997. ISSN 0748-4658 1533-3876. doi: 10.2514/2.5158.

[37] Jeong. Supersonic combustion on hydrogen fuel injection locations in a cavity-based combustor, 2008. See journal paper(Investigation of supersonic combustion with angled injection in a cavity-based combustor, JPP).

[38] Lig R. C. R. C. B. Billig and M. Lasky. A unified analysis of gaseous jet penetration. *AIAA Journal*, 9(6):1048–1058, 1971. ISSN 0001-1452. doi: 10.2514/3.49916. URL `http://dx.doi.org/10.2514/3.49916`.

[39] He Huang, Louis Spadaccini, and David Sobel. *Endothermic heat-sink of hydrocarbon fuels for scramjet cooling*. Joint Propulsion Conferences. American Institute of Aeronautics and Astronautics, 2002. doi: doi:10.2514/6.2002-387110.2514/6. 2002-3871. URL `http://dx.doi.org/10.2514/6.2002-3871`. doi:10.2514/6.2002-3871.

[40] S. H. Smith and M. G. Mungal. Mixing, structure and scaling of the jet in crossflow. *Journal of Fluid Mechanics*, 357:83–122, 1998. ISSN 00221120. doi: 10.1017/s0022112097007891.